NASA TECHNICAL NOTE

NASA TN D-5903

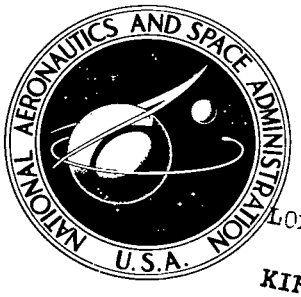




# EFFECTS OF ANGLE OF ATTACK AND BLUNTNESS ON THE HYPERSONIC FLOW OVER A 15° SEMIAPEX CONE IN HELIUM

*by Joseph W. Cleary and Charles E. Duller*

*Ames Research Center*
*Moffett Field, Calif. 94035*

NATIONAL AERONAUTICS AND SPACE ADMINISTRATION • WASHINGTON, D. C. • AUGUST 1970

| 1. Report No. | 2. Government Accession No. | 3. Recipient's Catalog No. |
|---|---|---|
| NASA TN D-5903 | | |

| 4. Title and Subtitle | 5. Report Date |
|---|---|
| EFFECTS OF ANGLE OF ATTACK AND BLUNTNESS ON THE HYPERSONIC FLOW OVER A 15° SEMIAPEX CONE IN HELIUM | August 1970 |
| | 6. Performing Organization Code |

| 7. Author(s) | 8. Performing Organization Report No. |
|---|---|
| Joseph W. Cleary and Charles E. Duller | A-3566 |
| | 10. Work Unit No. |
| 9. Performing Organization Name and Address | 129-01-09-07-00-21 |
| NASA Ames Research Center<br>Moffett Field, Calif. 94035 | 11. Contract or Grant No. |
| | 13. Type of Report and Period Covered |
| 12. Sponsoring Agency Name and Address | Technical Note |
| National Aeronautics and Space Administration<br>Washington, D. C. 20546 | 14. Sponsoring Agency Code |

15. Supplementary Notes

16. Abstract

Effects of angle of attack and bluntness on the hypersonic flow over a 15° semiapex cone were experimentally investigated for the limiting specific-heat ratio 1.67. Results are presented from wind-tunnel tests in helium at a free-stream Mach number of 14.9 and Reynolds number based on base radius of $0.86 \times 10^6$. Included are measurements of surface pressure and heat-transfer coefficients, shadowgraphs of shock-wave shape, and limiting streamlines adjacent to the surface. The tests spanned angles of attack from 0° to 30° and cone-bluntness ratios from 0 to 0.4. Comparisons of measurements with theory indicate generally good agreement.

| 17. Key Words (Suggested by Author(s)) | 18. Distribution Statement |
|---|---|
| angle of attack<br>surface pressure distribution<br>shock-wave shape<br>wind-tunnel tests in helium<br>effects of bluntness<br>comparisons with theory | Unclassified – Unlimited |

| 19. Security Classif. (of this report) | 20. Security Classif. (of this page) | 21. No. of Pages | 22. Price* |
|---|---|---|---|
| Unclassified | Unclassified | 44 | $3.00 |

*For sale by the Clearinghouse for Federal Scientific and Technical Information
Springfield, Virginia 22151

## SYMBOLS

| | |
|---|---|
| $C_p$ | pressure coefficient, $\left(\frac{p}{p_\infty} - 1\right) \frac{2}{\gamma M_\infty^2}$ |
| h | heat-transfer coefficient, $\frac{q}{T_r - T_w}$ |
| $h_o$ | stagnation-point heat-transfer coefficient |
| L | axial length of sharp cone |
| M | Mach number |
| p | pressure |
| q | heating rate |
| R | nose radius |
| Re | Reynolds number based on model base radius |
| $r_b$ | base radius of model |
| T | temperature |
| x,r,$\phi$ | body cylindrical coordinates ($\phi = 0°$ is the leeward ray) |
| $x_o$ | equivalent wind-axis coordinate |
| $\alpha$ | angle of attack |
| $\gamma$ | ratio of specific heats |
| $\delta$ | semiapex angle of cone |
| $\delta_o$ | equivalent-cone angle |
| $\theta_2$ | oblique-shock angle |
| $\nu$ | shear-line angle |
| $\sigma$ | flow angle |
| $\omega$ | angle of inclination to free stream |

## Subscripts

| | |
|---|---|
| 2 | at the shock but downstream |
| $\infty$ | free stream |
| r | recovery |
| w | wall |
| s | sharp cone |

# EFFECTS OF ANGLE OF ATTACK AND BLUNTNESS ON THE HYPERSONIC FLOW OVER A 15° SEMIAPEX CONE IN HELIUM

Joseph W. Cleary and Charles E. Duller

Ames Research Center

## SUMMARY

Effects of angle of attack and bluntness on the hypersonic flow over a 15° semiapex cone were experimentally investigated for the limiting specific-heat ratio 1.67. Results are presented from wind-tunnel tests in helium at a free-stream Mach number of 14.9 and Reynolds number of $0.86 \times 10^6$ based on the radius of the base. Included are measurements of surface pressure and heat-transfer coefficients, shadowgraphs of shock-wave shape, and limiting streamlines adjacent to the surface. The tests spanned a range of angles of attack from 0° to 30° and cone bluntness ratios from 0 to 0.4.

The results show that surface-pressure distribution and shock-wave shape of the sharp-cone are essentially conical. Bluntness not only destroys the conical nature of the surface pressure distribution and shock-wave shape, but also alters the flow-separation pattern on the lee side. Comparisons of theoretically predicted distributions of pressure and heat-transfer coefficients and shock-wave shape with experiment show generally good agreement.

## INTRODUCTION

Concern with problems of aerodynamic heating and performance during planetary atmospheric entry has given impetus to investigations of the effects of bluntness and angle of attack on the hypersonic characteristics of conical bodies. For the three-dimensional flows that are encountered during lifting entry, solutions to heating problems require knowledge of streamline characteristics as well as properties of the flow at the edge of the boundary layer (refs. 1 to 3). As a reasonable approximation for continuum flows, streamlines can be estimated by inviscid theory. The adequacy of inviscid theory to a specific case, however, is dependent on relative thicknesses of the boundary, entropy, and shock layers. It is apparent then that details of all properties of the flow including shock-layer thickness may have bearing on heating and performance estimates. How well inviscid theory approximates viscous flows can be assessed by comparison with experiment. While the adequacy of inviscid theory has been investigated for air (e.g., refs. 4 to 8 and others), investigations for other gases are meager.

The present investigation has a twofold purpose: (1) to present measurements that show effects of angle of attack and bluntness on the flow over a 15° semiapex cone for the limiting specific-heat ratio 1.67, and (2) to compare measurements with theory. Included are measurements of the distributions of surface pressure and heat-transfer coefficients, shock-wave shape, and limiting streamlines adjacent to the surface. Results were obtained from wind-tunnel tests in helium

at a Mach number of 14.9 and a Reynolds number based on model base radius of $0.86 \times 10^6$. The tests spanned a range of angles of attack from 0° to 30° and cone bluntness ratios from 0 to 0.4. The present investigation includes and supplements preliminary test results for helium given in references 7 and 8.

## EXPERIMENTAL METHOD

### Wind-Tunnel Facility

The tests were conducted in the Ames 20-Inch Hypersonic Tunnel in helium at a free-stream Mach number of 14.9. Reservoir temperature and pressure were, respectively, 545° R and 1250 psia, and the corresponding free-stream unit Reynolds number was $9.2 \times 10^6$ per foot. The wind-tunnel facility is a blowdown tunnel with an axisymmetric contoured nozzle and a 20-inch-diameter test section. The tunnel test section with the sharp-cone model mounted on the sting support is shown in figure 1. Operation of the wind tunnel is essentially automatic and the angle of attack can be varied from 0° to 30° at prescribed intervals by a controller programmed prior to the test. Further details of this facility are given in reference 9.

### Models and Test Procedure

The models were 15° semiapex sharp and blunt cones constructed from stainless steel. Their bluntness ratios were $R/r_b$ of 0 (sharp cone), 0.2, and 0.4. Pressure orifices and thermocouples were installed in separate models along a conical ray. Since only one ray was instrumented, tests at various circumferential angles $\phi$ were made by an axial rotation of the model. The axial positions of the pressure orifices and thermocouples and other details of the models are given in figure 2. Model surface pressures were measured with differential-pressure cells referenced to a known pressure. These cells measure pressure to an accuracy of about ± 0.02 psi. Surface temperatures of the models were measured with 40 gage chromel-constantan thermocouples that were spot welded to the inner surface of the models. Measurements of temperature are believed accurate to within ± 1° R.

Heat-transfer measurements were achieved by the transient temperature technique. Prior to a run the model was enclosed in a thin plastic cylindrical shroud that was supported at the upstream end by a tunnel starting probe, and at the downstream end by a ring attached to the sting behind the model. Cold gaseous nitrogen was bled into this leakproof shroud until the model surface temperature reached the desired level and was observed to be isothermal. After the tunnel started, the starting probe was retracted thereby rupturing the shroud and, in effect, instantaneously exposing the model to the free stream. As the model was heated, temperatures were measured at intervals of 0.2 second. Additional details of the heat-transfer test procedure and of the data reduction are given in reference 10.

## RESULTS AND DISCUSSION

### Experimental Results

*Pressure distribution*– Surface pressure distributions of the 15° cone are presented in figure 3 as functions of the sharp-cone axial coordinate $x_S/L$. From measurements of pressure and shock angle, the local Mach number on the windward stagnation line $\phi = 180°$ of the sharp cone was estimated to be about 1.46 at the highest angle of attack $\alpha = 30°$. Consistent with the fact that the flow was therefore locally supersonic for the entire angle-of-attack range of the test, $0 \leqslant \alpha \leqslant 30°$, figure 3(a) shows that except for a slight axial pressure gradient on the lee side, sharp-cone pressure distributions are essentially constant and the flow can be considered conical. Slight axial pressure gradients observable on the lee side are attributed to the low base pressure that was imposed on the leeward thickened boundary layer or separated flow. Figures 3(b) and 3(c) show that bluntness was sufficient to obliterate the essentially conical flow over the sharp cone. Here it can be seen that the characteristic overexpansion of the flow due to bluntness occurred for the range of angles of attack.

*Distributions of heat-transfer coefficient*– Figure 4 presents distributions of heat-transfer coefficient as a function of $x_S/L$. To demonstrate more clearly the effects of angle of attack and bluntness, results from figure 4 for $\phi = 0°$ and 180° are replotted in figure 5 using logarithmic scales. For $\alpha = 0°$ comparisons are made with similarity theory to show that the boundary layer was laminar. For $R/r_b = 0$ a straight line with slope of –0.5 has been faired through the data to illustrate agreement with flat-plate theory. The results for $R/r_b = 0.2$ and 0.4 are compared with laminar similarity theory of reference 11. Because of the reasonably good agreement with theory, it is concluded that the flow was laminar for the range of bluntness.

For $\alpha > 0°$, reference 12 predicts that as at $\alpha = 0°$, the sharp-cone distributions of h on the windward stagnation line are straight lines with slopes of –0.5 if the flow is laminar. Figure 5 shows that for $R/r_b = 0$, experiment conforms well with this prediction except at $x_S/L = 0.12$ for $\alpha \geqslant 10°$ where measurements of h appear low. The disagreement with theory for this condition is not clearly understood, but may be due to heat-conduction effects that become more severe with increasing $\alpha$ and with proximity to the cone apex. Windward distributions of h for $R/r_b = 0.2$ and 0.4 are also believed laminar in view of the prevailing decreases of h with $x_S/L$. The leeward distributions of h for small $\alpha$ appear laminar also; however, at large angles of attack departures from laminar type distributions indicate transition of the flow.

From figure 5 it can be seen that maximums occurred in the distributions of h for $R/r_b = 0.2$ and $\alpha = 15°$ and 30°. These maximums, in general, resemble maximums in heating-rate distributions reported in reference 13 from tests in air for about the same bluntness ratio. However, in the present case the maximums are not well defined and may be influenced by heat conduction owing to proximity of the nose.

*Surface flow*– Views of limiting streamlines as indicated by white streaks of an oil and titanium oxide mixture are presented in figure 6.[1] The lee, side, and windward views are shown

[1] The three white lines visible in figure 6 denote 30° sectors symmetrically disposed with respect to the windward stagnation line.

normal to the conical surface while the front view is along the cone axis. Figure 6 shows that on the lee side there is an accumulation of the white oxide mixture in regions where the pressure and shearing forces adjacent to the surface are low. For small $\alpha$ the flow is not necessarily separated and an accrual of the white oxide mixture is believed more indicative of a thickened boundary layer. On the other hand, for large $\alpha$, separation is indicated along two lines, one from the windward flow and the other from a weaker flow on the lee side, to form deposits in sectors that are symmetrically disposed.

The sharp-cone separation patterns closely resemble patterns of incompressible flow separation presented in reference 14. Results from reference 14 show that flow separation on sharp cones is associated with a complicated arrangement of vortices that form on the lee side. In the present case, the separated flow region is well within the lee shielded region of the flow. Measurements indicate that for the sharp cone $\phi_{shielded}/\phi_{separation}$ were 1.4 and 1.6 for respective angles of attack of 20° and 30°.

For $\alpha = 10°$ and $R/r_b = 0$ figure 6 shows heavy streaks of oil formed downstream of the apex along lines paralleling the leeward deposit. These streaks are like those reported in reference 15 from tests in air. The heavy lines are superimposed on and appear to originate from lighter striations that are inclined at steeper angles to cone elements. The lighter striations indicate direction of the normal laminar flow. This detail is shown more clearly in figure 7 from tests in air at $M_\infty = 10.6$. Similar flow patterns were observed over rotating disks and swept wings in reference 16 where heavy lines that formed were attributed to vortices that develop in three-dimensional boundary layers. Furthermore, reference 17 reports vortex streaks appearing in the wakes of inclined conical type bodies. These vortices preceded development of turbulent flow, and the vortex axes tended to aline with the direction of external streamlines adjacent to the boundary layer. In like manner for the present case, although not shown, estimates of streamline directions for the sharp cone by Newtonian theory (ref. 13) agree well with the projections of heavy lines shown in the front view of figure 6. Increasing the angle of attack or bluntness appears to have a mitigating effect on the formation of the heavy lines (see fig. 6). In addition, increasing bluntness increases the angle of the normal laminar flow to cone elements in conformance with results from tests in air given in reference 13.

*Shock-wave shape*– Shadowgraph profiles of shock waves that show the effects of angle of attack and bluntness are presented in figure 8. Here it can be seen that for $0° \leqslant \alpha \leqslant 30°$ the sharp-cone shocks are essentially straight even on the lee side where the flow separated at the higher angles of attack. Also, a white shear line can be seen in the leeward shock layer of the sharp cone that demarcates the inner thickened boundary layer or separated flow from the external essentially inviscid flow. Pitot-pressure measurements of reference 18 show that for $\phi = 0°$ the inner layer has low kinetic energy. While the shear line appears straight, it is actually slightly curved, indicating that the viscous region of the flow was not truly conical.

In the absence of a visible shear line, bluntness appears to have an alleviating effect on flow separation. However, the surface flow shown in figure 6 and pitot-pressure measurements of reference 18 indicate flow separation at a distance downstream of the nose. On the windward side the inflection point of the blunt-cone shock moved forward with increasing $\alpha$. For $\alpha = 30°$ figure 8 shows that the windward shock retains a slight inflection even though the flow in the shock layer is subsonic (see figs. 3(b) and 3(c)). In addition it can be seen by comparison with the sharp-cone shock that at the cone base, the displacement of the blunt-cone shock and the shock angle has closely approached that of the sharp cone.

## Comparisons With Theory

Initially, comparisons will be made of sharp-cone experimental results with theory; then comparisons will be made for the blunt cone.

*Sharp cone*– Experimental results of the sharp cone are compared with various theoretical estimates in figures 9 to 13. A comparison of windward stagnation-line pressure at a representative axial position, $x_s/L = 0.36$, with inviscid theories is shown in figure 9 for a range of $\omega$ from 15° to 45°. While this range of $\omega$ probably exceeds that for which thin-shock layer (ref. 19) and linearized characteristics (ref. 20) theories apply, results are compared, nevertheless, for interest.

The estimates of pressure by linearized-characteristics theory were made to second order. Tangent-cone pressures were estimated from exact inviscid solutions while thin-shock-layer estimates are from equations given in reference 19 with corrections given in reference 21. The swept-cylinder pressures were calculated by exact relations from simple sweep theory. This theory can be considered a lower bound on stagnation-line pressures of conical flows as borne out by the comparison shown in figure 9.

Except for swept-cylinder theory, figure 9 shows generally good agreement between experiment and the various other theories within the limited range, $15° \ll \omega \ll 30°$. For large inclinations $\omega \to 45°$ linearized-characteristics, tangent-cone, and thin-shock-layer theories all overestimate experiment, and of the various theories shown, only Newtonian agrees closely with experiment. This is partly fortuitous for this particular cone angle, however, since it can be shown that for a specified $\omega$, experiment should agree better with swept-cylinder theory as $\delta \to 0°$ and with tangent-cone theory as $\alpha \to 0°$.

The windward shock angle $\theta_2$, and the angular difference $(\theta_2 - \omega)$ are shown as functions of $\omega$ and compared with inviscid theories in figure 10. Shock angles were measured from shadowgraphs of figure 8 with corrections applied for the slight optical distortion that is evident from the rectangular appearance of the square grid. Of the various theories shown, linearized characteristics theory appears to give the best estimate of shock angle. It is of interest that the measured angular difference $(\theta_2 - \omega)$ initially decreases and then increases with increasing $\omega$. The initial decrease may be a viscous effect since this trend is not predicted by linearized characteristics theory or by exact inviscid solutions for air from reference 22 that are not shown.

A comparison of the windward-pressure ratio, $p/p_2$, as a function of $\omega$ with various theories is shown in figure 11. This ratio was calculated from the measured pressures and shock angles and is, therefore, subject to the inaccuracies of both measurements. None of the theories adequately predicts the trend of experiment with increasing $\omega$. Although not shown, exact inviscid theory for air (ref. 22) predicts that at least for $\alpha < \delta$, $p/p_2$ increases very slightly with increasing $\omega$. In figure 11 a greater increase with increasing $\omega$ is indicated by experiment and this may be a viscous effect. Nevertheless, the upper bound given by swept-cylinder theory was not exceeded by experiment.

Comparisons of circumferential distributions of pressure with inviscid theories are shown in figure 12 for $\alpha = 10°$ and 20°. All of the theories shown appear to predict adequately the circumferential distribution of pressure for $\alpha = 10°$ except on the lee side where the theories underestimate pressure. For $\alpha = 20°$ Newtonian theory gives the best estimate on the more

windward side. On the lee side, the pressure minimum predicted by linearized-characteristics and thin-shock-layer theories is less than vacuum $C_p = -(2/\gamma M_\infty^2)$ and it appears that for $\alpha = 20°$ the applicable angle-of-attack range of these theories is exceeded. A pressure minimum was not distinctly observed experimentally even though (as indicated by surface flow results from fig. 6(a)) separation did not occur for $\phi \gtrsim 30°$.

On the lee side experimental results are summarized as functions of the leeward inclination in figure 13 in lieu of theory. The experimental pressure curve (fig. 13(a)) was obtained from extrapolations of pressures given in figure 3(a) to $x_S/L = 0$. These results are compared with oblique-shock estimates of pressure from measured shock-wave angles. The shock angle, $\theta$, and shear-line angle, $\nu$, shown in figure 13(b) were measured at the apex from shadowgraphs (fig. 8), and the flow angle at the shock $\sigma_2$ was estimated by oblique-shock theory. Since $\sigma_2$ is slightly less than $\nu$, a compression of the flow is indicated across the shock layer. It is clear, however, from figure 13(a) that the increase of pressure was generally small across the lee shock layer.

The measured distribution of heat-transfer coefficient of the sharp cone for $\alpha = 0°$ is compared in figure 14 with flat-plate reference-enthalpy theory (ref. 23) modified by Mangler's factor $\sqrt{3}$. Figure 14 shows good agreement between reference enthalpy theory and present experimental results.

*Blunted cone*— Measured pressures as a function of the axial distance from the nose x/R for $R/r_b = 0.2$ and 0.4 are compared in figure 15 with two inviscid theories at $\alpha = 0°$, 10°, and 20°. The measured pressures for both bluntness ratios agree well with each other as functions of x/R and $\phi$. With minor exceptions on the lee side, good agreement is shown with inviscid theory by the three-dimensional method of characteristics program of reference 8. For $\alpha = 20°$ this theory yielded results for $x/R \lesssim 9.5$ but because numerical difficulties were encountered as $p \to 0$ at $\phi \sim 30°$, results were unobtainable for greater x/R.

The equivalent-body theory shown in figure 15 is a tangent-cone approximation that utilizes axisymmetric solutions to account for variations of pressure with x/R and $\phi$. This method can be used to give a fair estimate of pressure distribution where more rigorous methods may encounter numerical difficulties. In order to select the appropriate pressure from the axisymmetric solutions, it is necessary to transform the body axis coordinates x/R and $\phi$ to the corresponding $x_O/R$ coordinate and cone angle of the axisymmetric solutions. The analogous axisymmetric cone angle $\delta_O$ is evaluated from equation (1)

$$\sin \delta_O = \sin \delta \cos \alpha - \cos \delta \sin \alpha \cos \phi \tag{1}$$

and the corresponding value of $x_O/R$ is given by equation (2).

$$\frac{x_O}{R} = \left[\left(\frac{x}{R} - 1\right) \cos \alpha + 1\right] + \left[\left(\frac{x}{R} - 1\right) \sin \delta + 1\right] \frac{\sin \alpha}{\cos \delta} \cos \phi \tag{2}$$

The equivalent-body theory shown in figure 15 was estimated from axisymmetric solutions given in figure 16. Figure 15 shows that equivalent-body theory, similar to the tangent-cone approximation for the sharp cone, tends to overestimate windward pressure and underestimate leeward pressure.

In figure 17 shock-wave shape is compared with three-dimensional characteristics theory. The close agreement shown between experiment and theory for both leeward and windward shocks indicates that viscous effects on shock shape were small.

A comparison of the distribution of heat-transfer coefficient normalized by the theoretical stagnation-point value with similarity theory (ref. 11) is shown in figure 18 for $\alpha = 0°$. Similar comparisons for $\alpha > 0°$ using a simplified method given in reference 3 for applying similarity theory at angle of attack are shown in figure 19. The stagnation-point heat-transfer coefficients were estimated from reference 24 using a blunt-body solution of the flow (ref. 25) to evaluate the stagnation-point velocity gradient. The theoretical estimates of $h/h_o$ in figures 18 and 19 were made using measured pressure distributions presented in figures 3(b) and 3(c). For $\alpha = 0°$, figure 18 shows good agreement between theory and experiment for both bluntness ratios. Similar agreement is shown in figures 19(a) and 19(b) for $\alpha = 5°$ and 10°, respectively; but for higher angles of attack, theory tends to underestimate the measured heating. Since theory does not account for increases in h due to the effects of entropy gradients or cross flow, the differences shown at higher angles of attack may be due, in part, to these effects.

## CONCLUDING REMARKS

Experimental results presented for the limiting specific-heat ratio 1.667 show effects of angle of attack and bluntness on the hypersonic flow over a 15° semiapex cone. The results from tests at angle of attack demonstrate that surface pressure and shock-wave shape of the sharp cone are essentially conical. Bluntness obliterates the essentially conical pressure distribution and shock shape of the sharp cone and alters the flow separation pattern on the lee side by promoting flow attachment adjacent to the nose.

Measured pressure distributions and shock shapes of the blunted cone are predicted well for $\alpha \geqslant 0°$ by inviscid numerical solutions of the flow. Deficiencies of less rigorous theories are demonstrated by comparisons with sharp-cone results. Similarity theory for laminar boundary layers appears to predict adequately the measured distributions of heat-transfer coefficient.

Ames Research Center
National Aeronautics and Space Administration
Moffett Field, Calif., 94035, April 1, 1970

## REFERENCES


1. Vaglio-Laurin, R.: Laminar Heat Transfer on Blunt-Nosed Bodies in Three-Dimensional Hypersonic Flow. WADC–TN–58–147, Polytechnic Inst. of Brooklyn, May 1958.

2. Pasiuk, Lionel: Comparisons of Experimental and Theoretical Heat Transfer to a Yawed Sphere-Cone Model at Supersonic Speeds. NOLTR 63–208, Aerodynamics Res. Rep. 207, Oct. 1964.

3. De Jarnette, Fred R.; and Davis, Ruby M.: A Simplified Method for Calculating Laminar Heat Transfer Over Bodies at an Angle of Attack. NASA TN D–4720, 1968.

4. Jones, D. J.: Numerical Solutions of the Flow Field for Conical Bodies in a Supersonic Stream. NRC–10361; NAE–LR–507, National Aeronautical Establishment, Ottawa, Canada, July 1968.

5. Chan, Y. Y.: An Experimental Study of a Yawed Circular Cone in Hypersonic Flows. AIAA J., vol. 7, no. 10, Oct. 1969, pp. 2035–2037.

6. Cleary, Joseph W.: An Experimental and Theoretical Investigation of the Pressure Distribution and Flow Fields of Blunted Cones at Hypersonic Mach Numbers. NASA TN D–2969, 1965.

7. Cleary, Joseph W.: Effects of Angle of Attack and Nose Bluntness on the Hypersonic Flow Over Cones. AIAA Paper 66–414, 4th Aerospace Sciences Meeting, June 27–29, 1966.

8. Rakich, John V.; and Cleary, Joseph W.: Theoretical and Experimental Study of Supersonic Steady Flow Around Inclined Bodies of Revolution. AIAA Paper 69–187, 7th Aerospace Sciences Meeting, Jan. 20–22, 1969.

9. Tendeland, Thorval; and Pearson, Douglas B., Jr.: Effectiveness of Two Flap Controls on a Mercury Type Capsule at a Mach Number of 15 in the Ames Hypersonic Helium Tunnel. NASA TM X–660, 1962.

10. Marvin, Joseph G.: Pressure and Heat-Transfer Distribution on the Afterbody of a Lifting Mercury-Type Capsule at Mach Number 15 in Helium. NASA TM X-783, 1963.

11. Lees, L.: Laminar Heat Transfer Over Blunt-Nosed Bodies at Hypersonic Flight Speeds. Jet Propulsion, vol. 26, no. 4, April 1956, pp. 259–269, 274.

12. Reshotko, Eli: Laminar Boundary Layer With Heat Transfer on a Cone at Angle of Attack in a Supersonic Stream. NACA TN 4152, 1957.

13. Cleary, Joseph W.: Effects of Angle of Attack and Bluntness on Laminar Heating-Rate Distributions of a 15° Cone at a Mach Number of 10.6. NASA TN D–5450, 1969.

14. Rainbird, W. J.; Crabbe, R. S.; and Jurewicz, L. S.: A Water Tunnel Investigation of the Flow Separation About Circular Cones at Incidence. NRC–7633; NAE–LR–385, National Aeronautical Establishment, Ottawa, Canada, Sept. 1963.

15. McDevitt, John B.; and Mellenthin, Jack A.: Upwash Patterns on Ablating and Nonablating Cones at Hypersonic Speeds. NASA TN D–5346, 1969.

16. Gregory, N.; Stuart, J. T.; and Walker, W. S.: On the Stability of Three-Dimensional Boundary Layers With Application to the Flow Due to a Rotating Disk. Phil. Trans. Roy. Soc. (London), Ser. A., vol. 248, no. 943, July 1955, pp. 155–199.

17. Seiff, Alvin; and Wilkins, Max E.: Experimental Investigation of a Hypersonic Glider Configuration at a Mach Number of 6 and at Full-Scale Reynolds Numbers. NASA TN D–341, 1961.

18. Cleary, Joseph W.: Effects of Angle of Attack and Bluntness on the Shock-Layer Properties of a 15° Cone at a Mach Number of 10.6. NASA TN D–4909, 1968.

19. Cheng, H. K.: Hypersonic Shock-Layer Theory of a Yawed Cone and Other Pointed Bodies. J. Fluid Mech., vol. 12, no. 2, Feb. 1962, pp. 169–191.

20. Rakich, John V.: Numerical Calculation of Supersonic Flows of a Perfect Gas Over Bodies of Revolution at Small Angles of Yaw. NASA TN D–2390, 1964.

21. Sapunkov, Y. G.: Hypersonic Flow Around a Circular Cone at an Angle of Attack. NASA TT F–8414, 1963.

22. Jones, D. J.: Tables of Inviscid Supersonic Flow About Circular Cones at Incidence $\gamma = 1.4$. Part II, AGARDograph 137, 1969.

23. Eckert, E. R. G.: Engineering Relations for Heat Transfer and Friction in High-Velocity Laminar and Turbulent Boundary-Layer Flow Over Surfaces With Constant Pressure and Temperature. Trans. ASME, vol. 68, no. 6, Aug. 1956, pp. 1273–1283.

24. Fay J. A.; and Riddell, F. R.: Theory of Stagnation Point Heat Transfer in Dissociated Air. J. Aero. Sci., vol. 25, no. 2, Feb. 1958, pp. 73–85, 121.

25. Inouye, Mamoru; and Lomax, Harvard: Comparison of Experimental and Numerical Results for the Flow of a Perfect Gas About Blunt-Nosed Bodies. NASA TN D–1426, 1962.

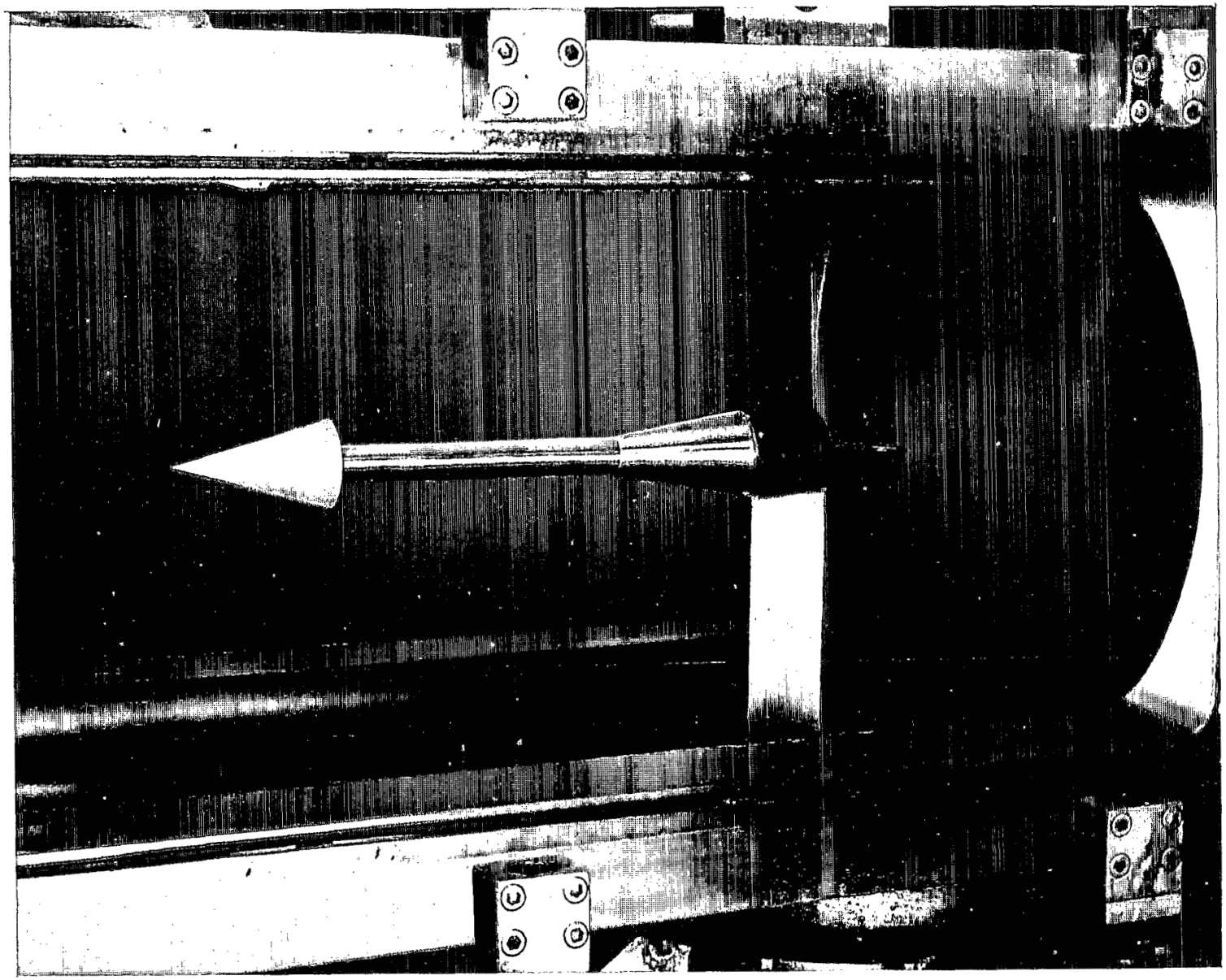

Figure 1.-- Sharp-cone model mounted in the 20-inch hypersonic helium tunnel.

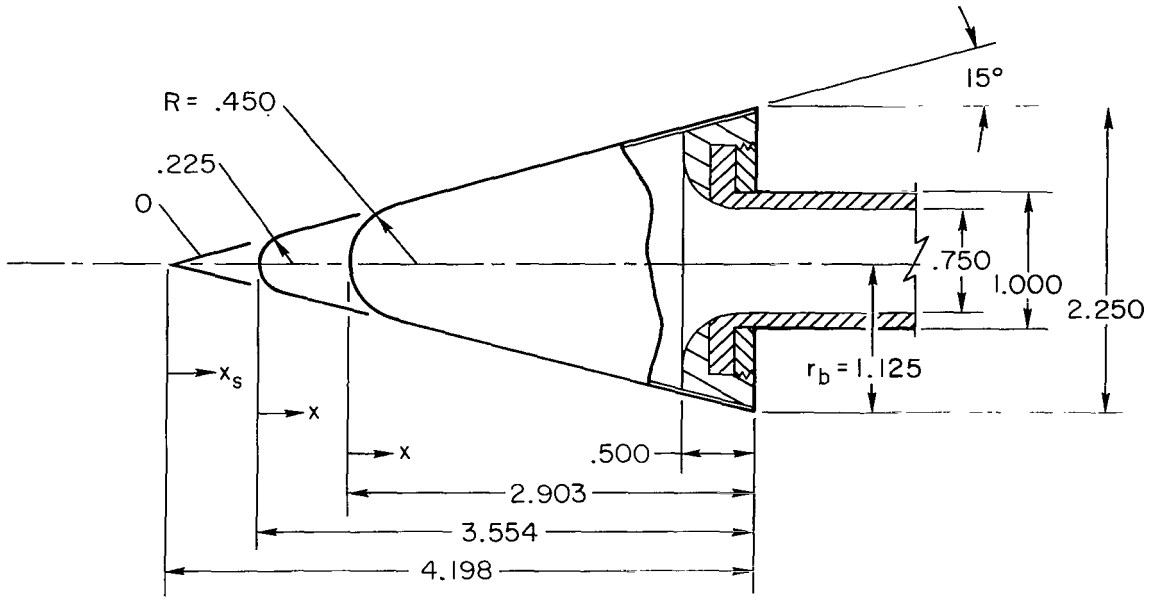


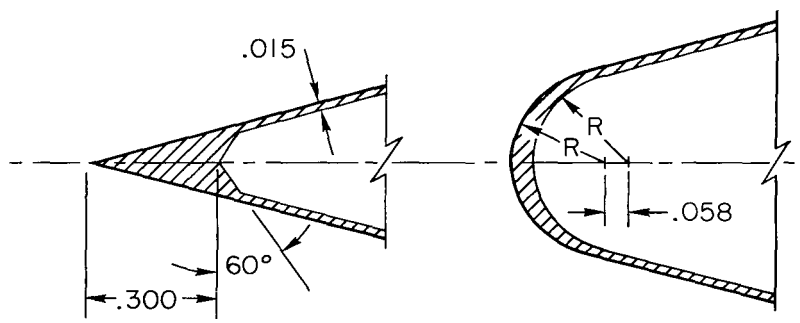


Detail of noses

| Pressure orifice and thermocouple locations | | | | |
|---|---|---|---|---|
| $R/r_b = 0$ | $R/r_b = 0.2$ | | $R/r_b = 0.4$ | |
| $x_s/L$ | x/R | $x_s/L$ | x/R | $x_s/L$ |
| 0.119* | 1.000* | 0.207 | 0.741 | 0.387 |
| .238 | 2.000 | .261 | 1.000 | .415 |
| .357 | 3.000 | .314 | 1.500 | .468 |
| .477 | 4.000 | .368 | 2.000 | .522 |
| .596 | 6.000 | .476 | 3.000 | .629 |
| .715 | 8.000 | .583 | 4.000 | .736 |
| .834 | 10.000 | .690 | 5.000 | .844 |
| | 12.000 | .797 | | |

* Thermocouple only
Note: All dimensions in inches

Figure 2.– Dimensional details of the models.

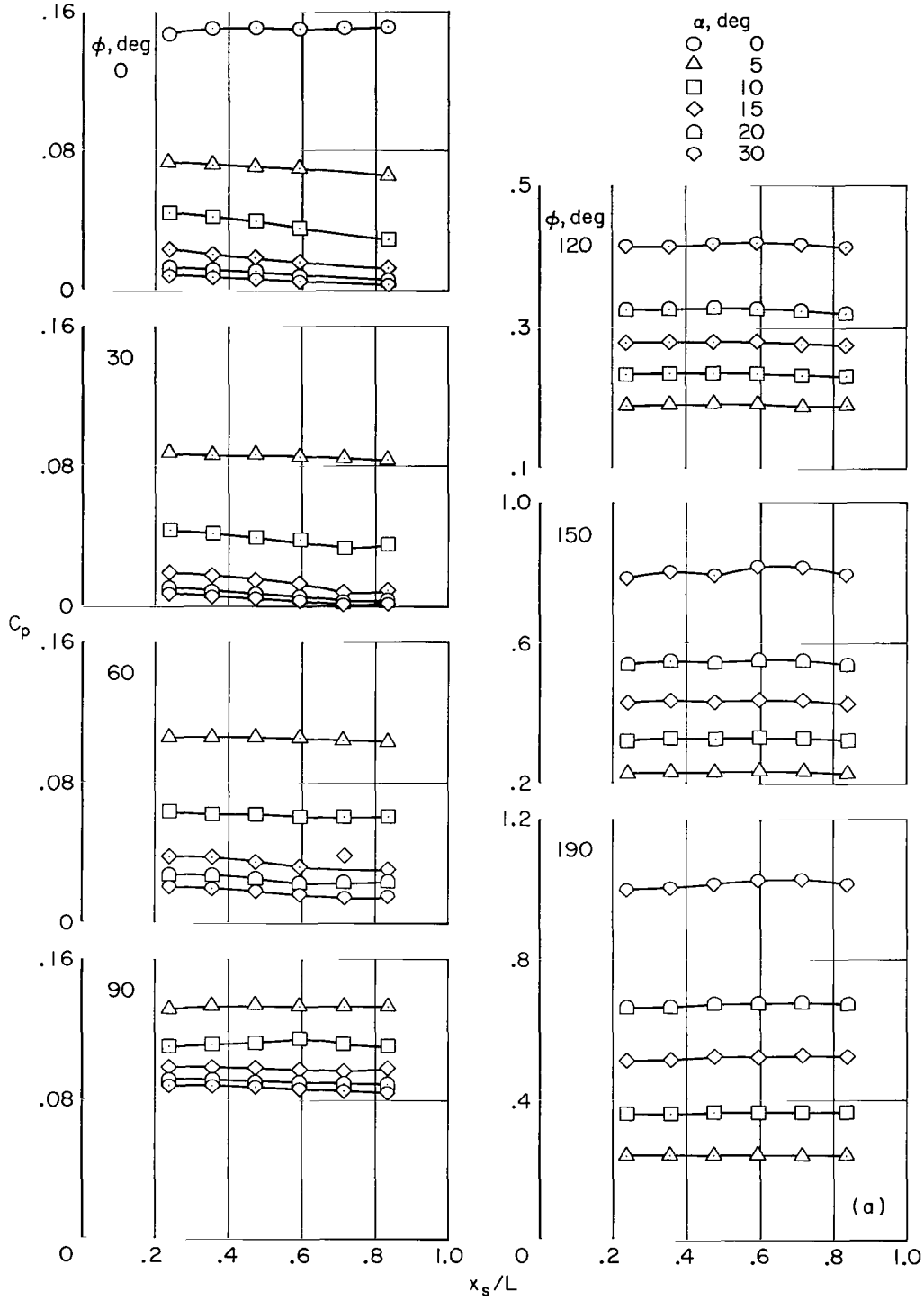


(a) $R/r_b = 0$

Figure 3.– Surface pressure distribution; $M_\infty = 14.9$, $Re_\infty = 0.86 \times 10^6$.

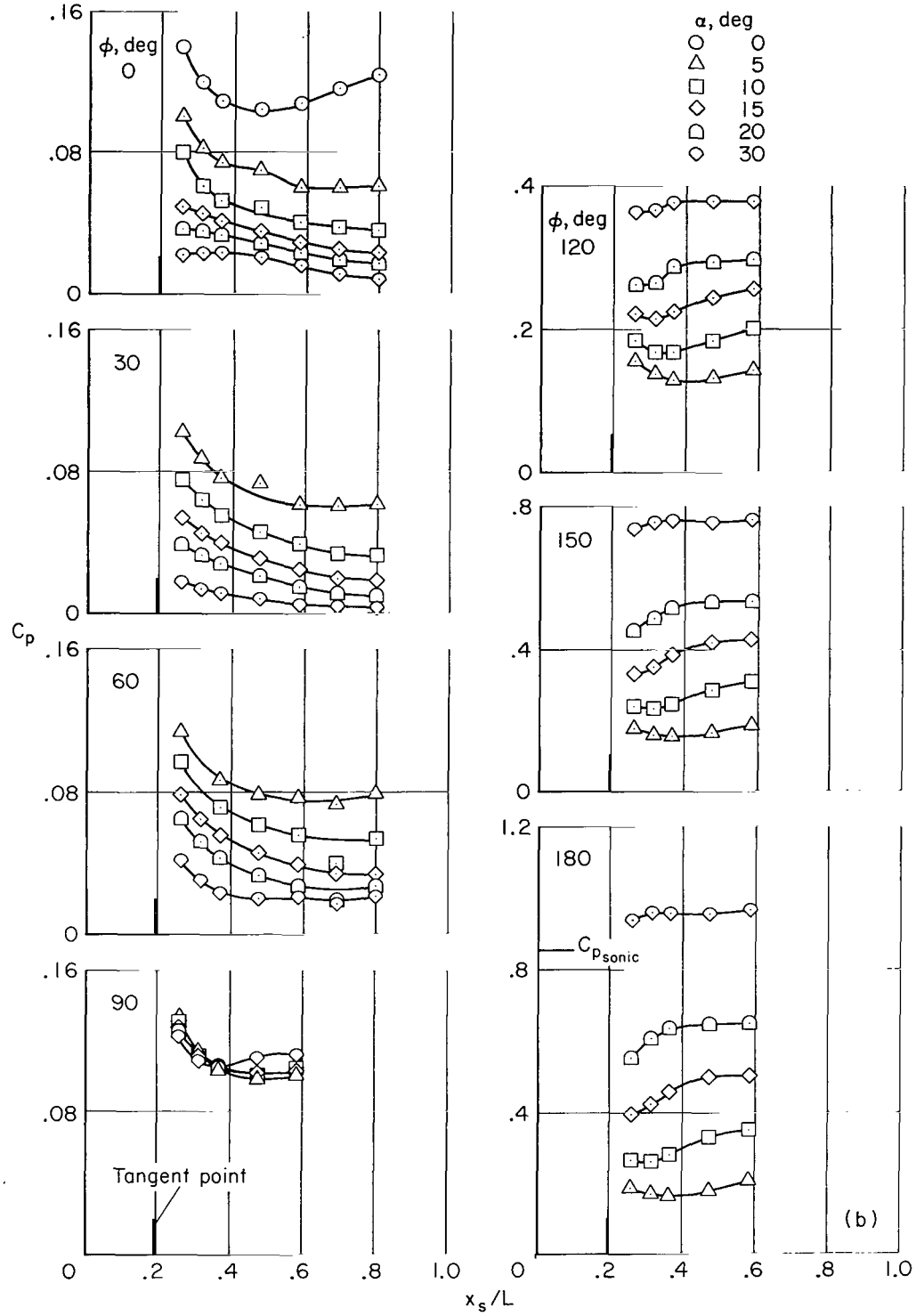


(b) $R/r_b = 0.2$

Figure 3.– Continued.

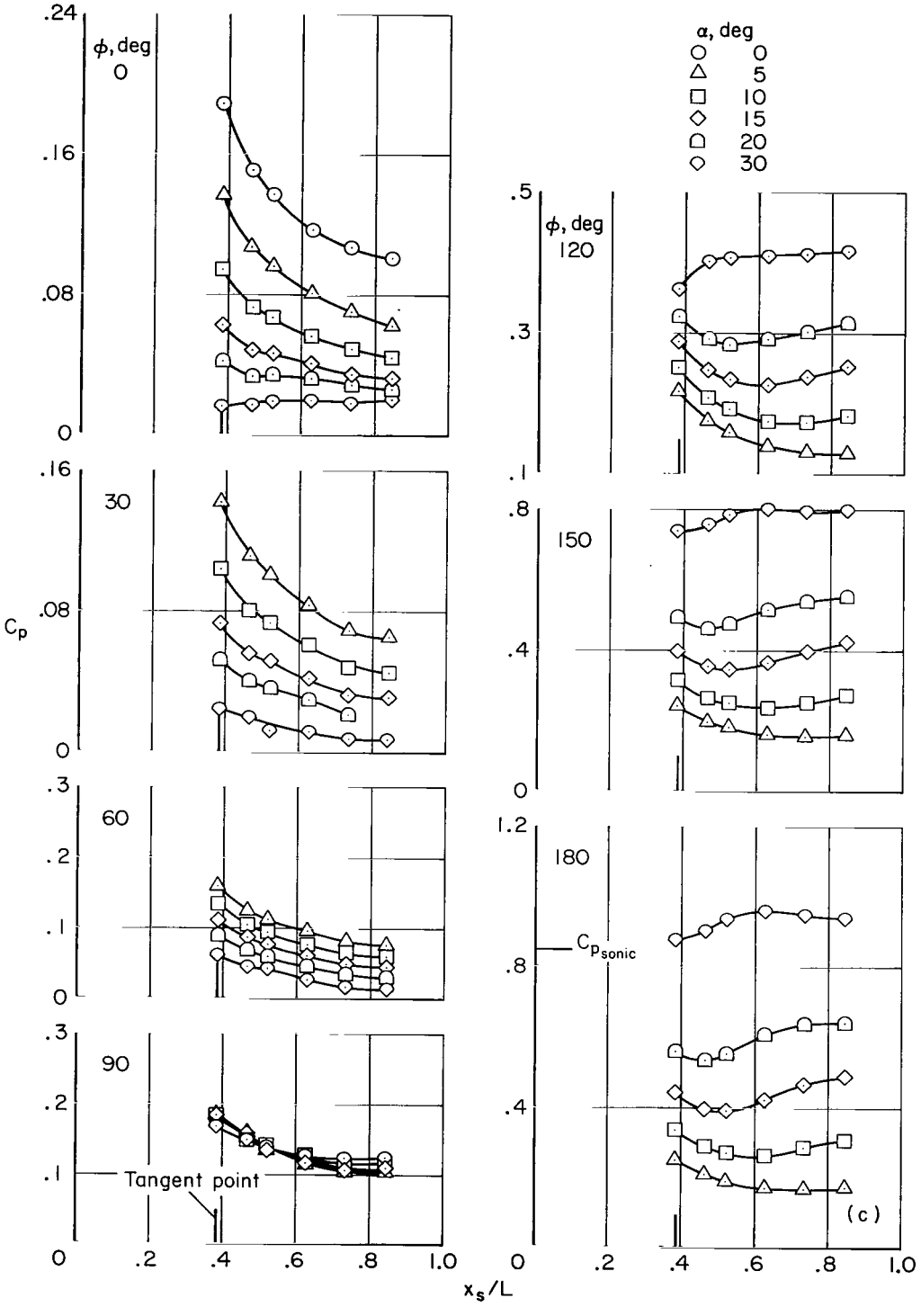


(c) $R/r_b = 0.4$

Figure 3.– Concluded.

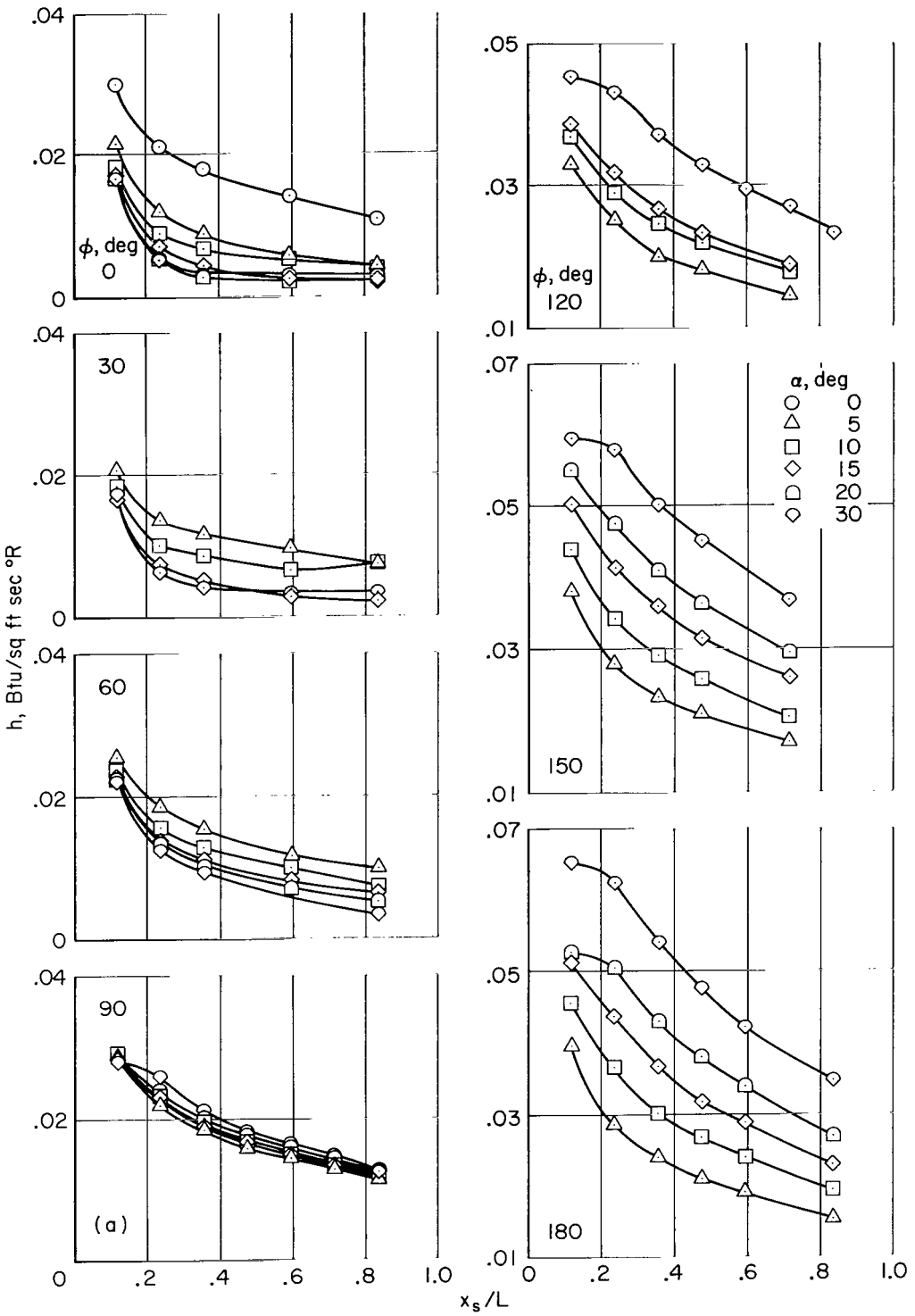


(a) $R/r_b = 0$

Figure 4.– Distributions of heat-transfer coefficient; $M_\infty = 14.9$, $Re_\infty = 0.86 \times 10^6$.

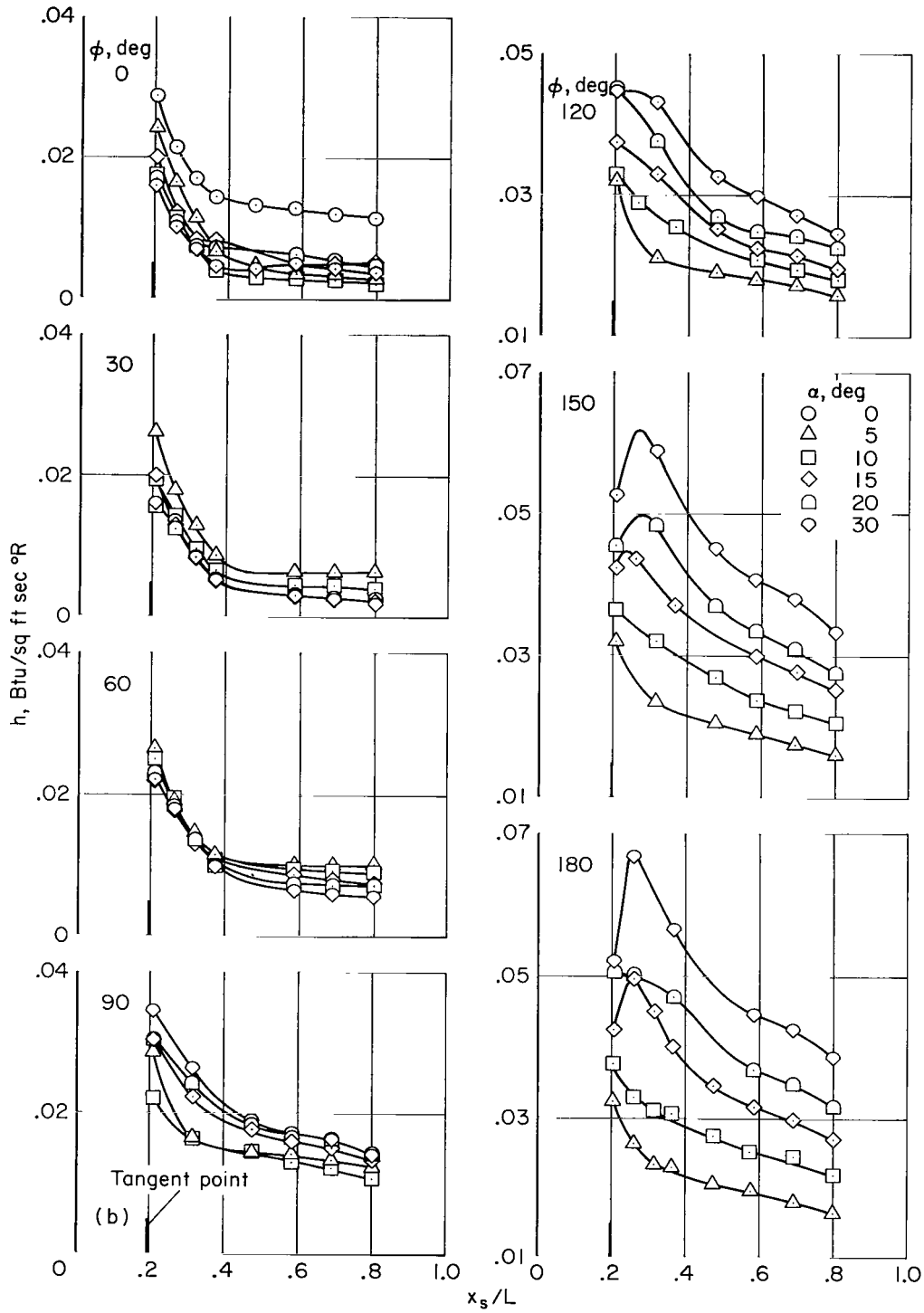


(b) $R/r_b = 0.2$

Figure 4.– Continued.

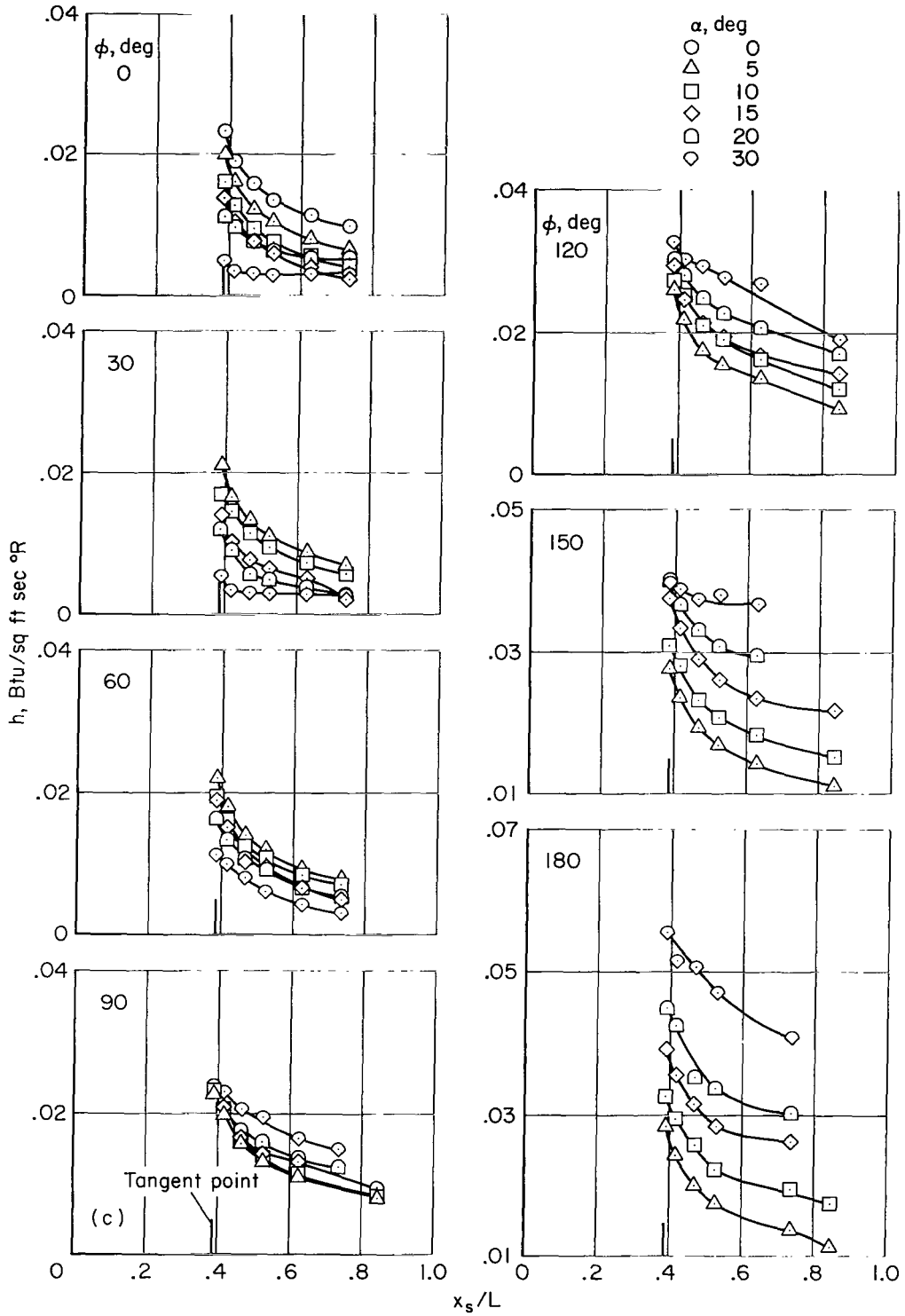


(c) $R/r_b = 0.4$

Figure 4.– Concluded.

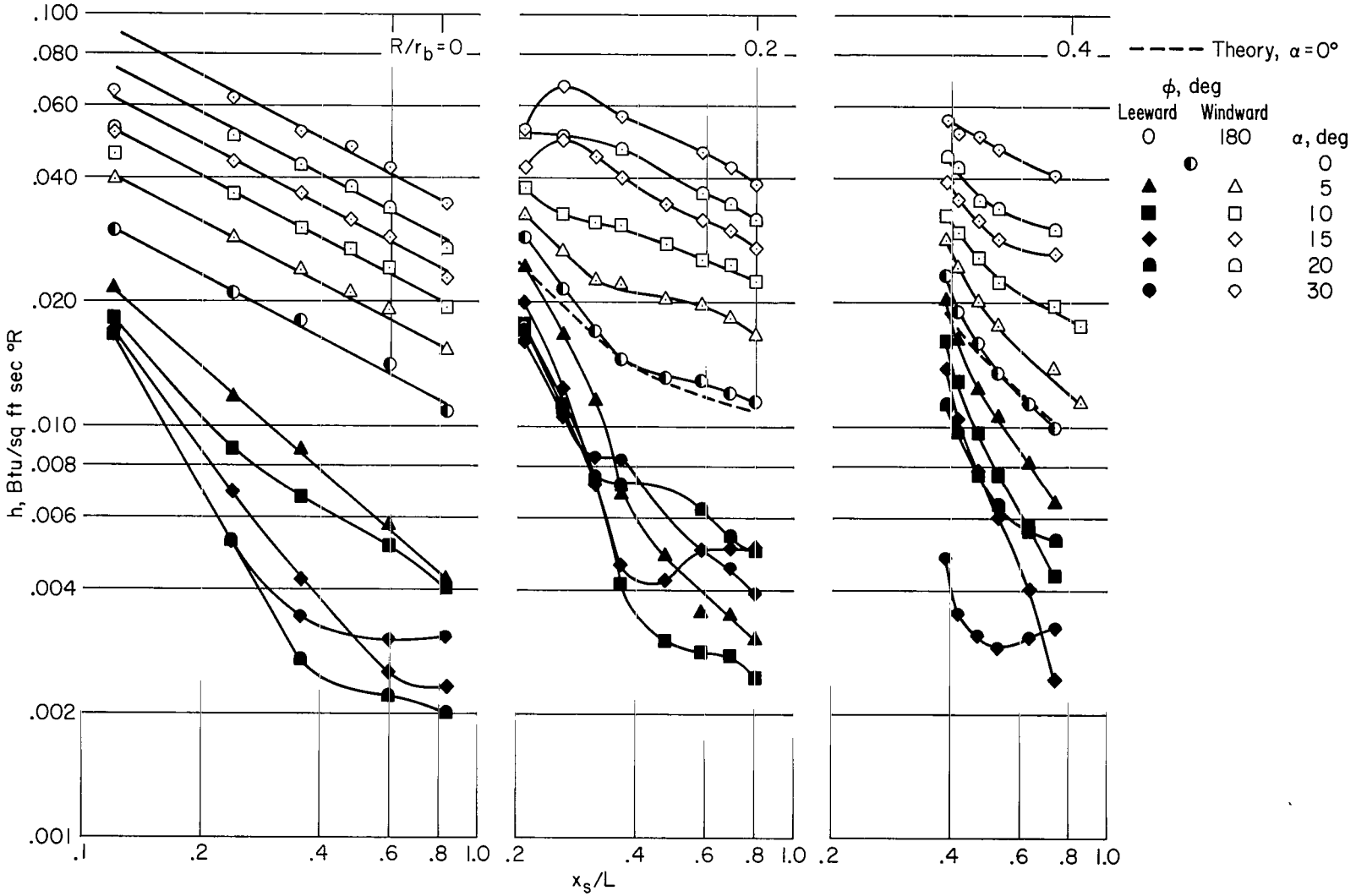


Figure 5.– Effects of angle of attack and bluntness on the distribution of heat-transfer coefficient; $M_\infty = 14.9$, $Re_\infty = 0.86 \times 10^6$.

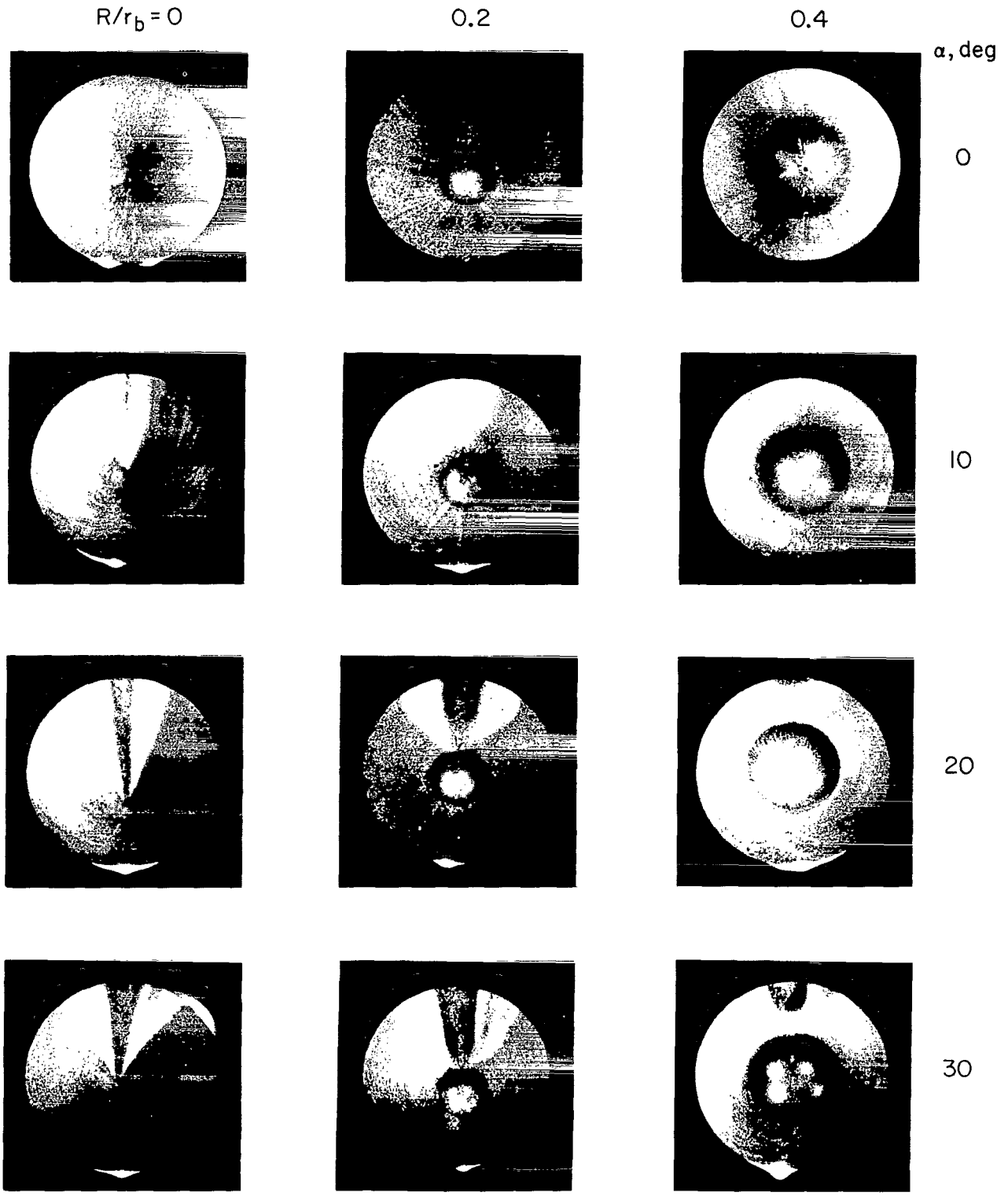


(a) Front view.

Figure 6.– Effects of angle of attack and bluntness on surface flow; $M_\infty = 14.9$, $Re_\infty = 0.86 \times 10^6$.

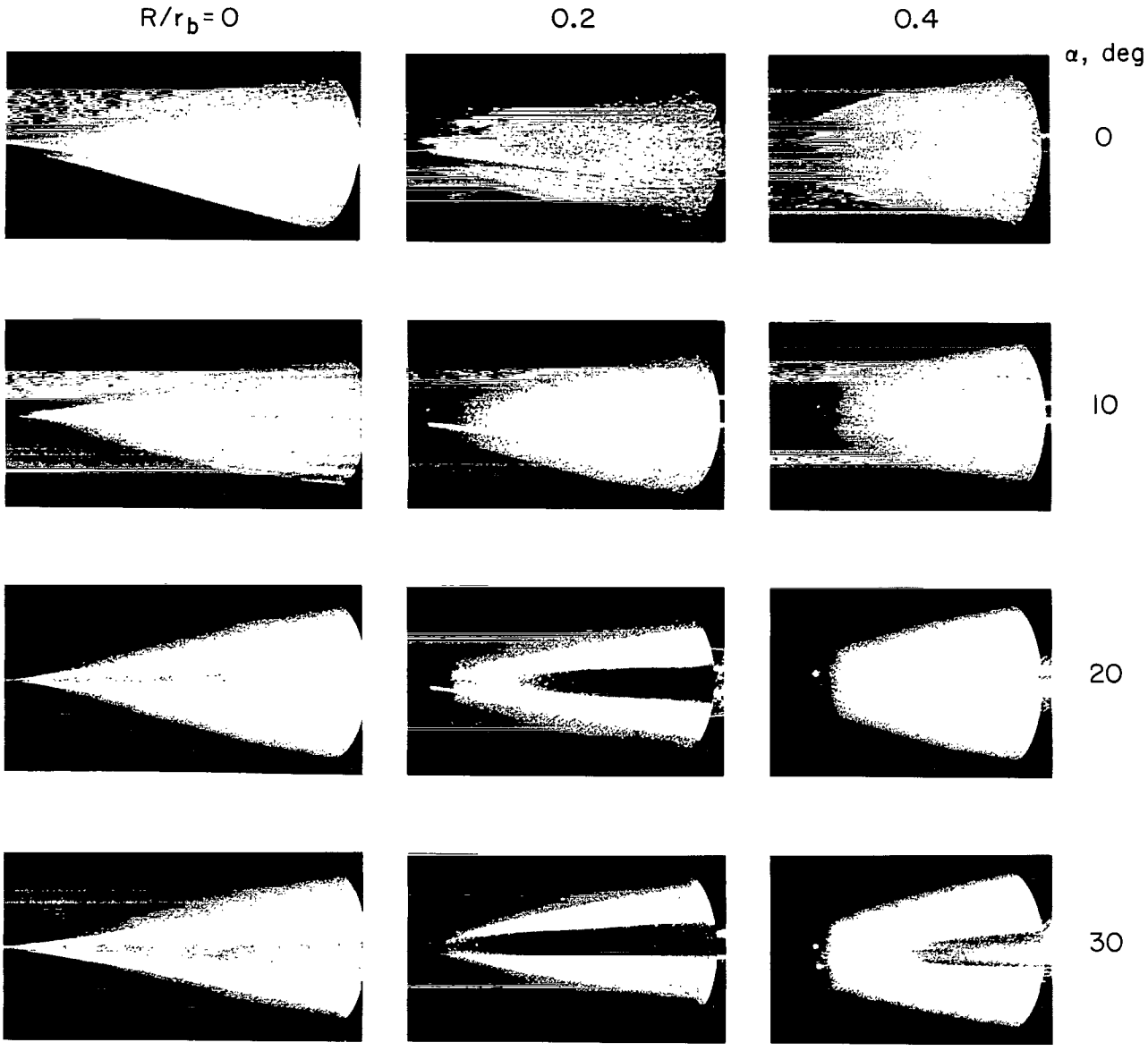


(b) Leeward view.

Figure 6.– Continued.

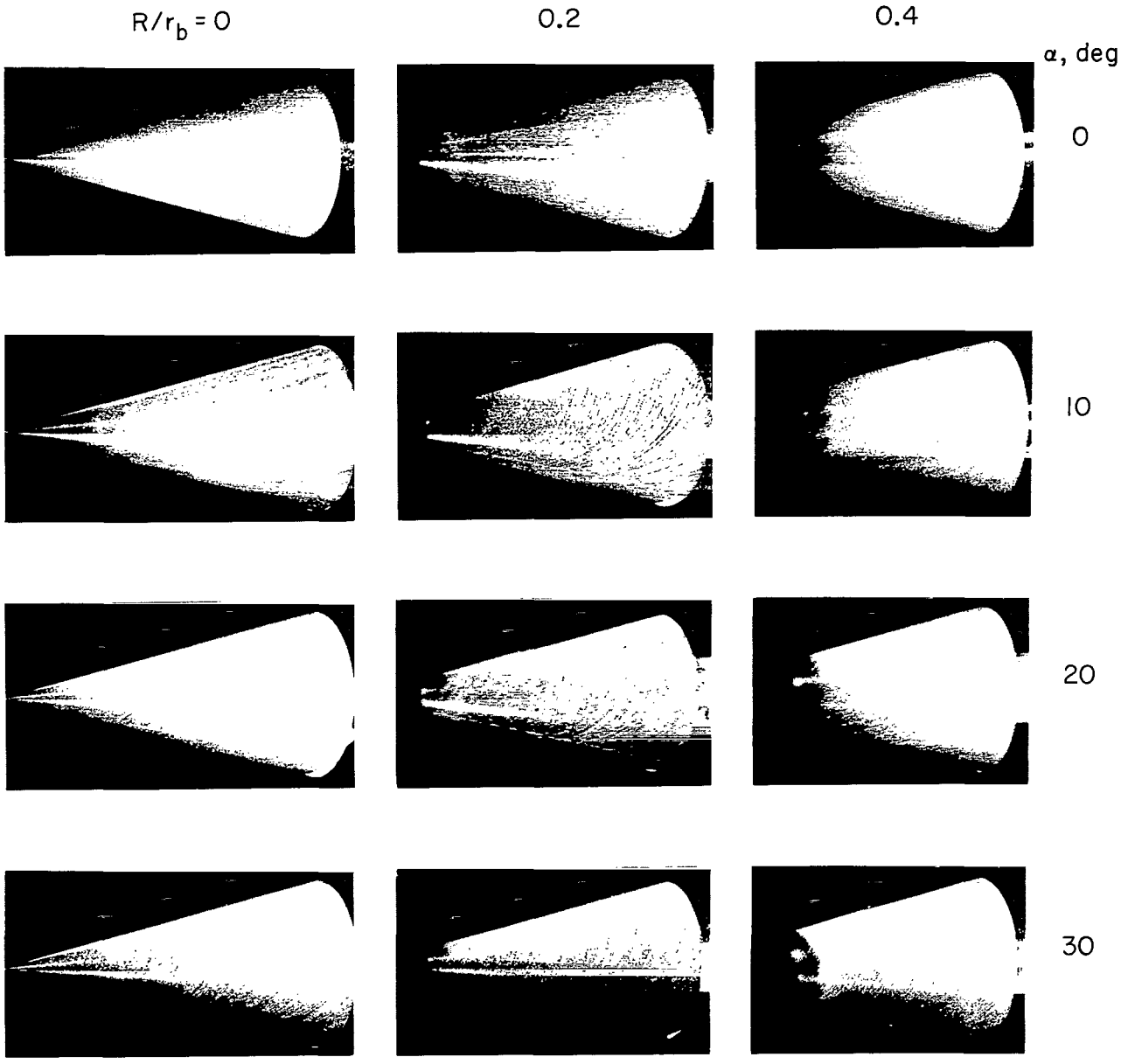


(c) Side view.

Figure 6.– Continued.

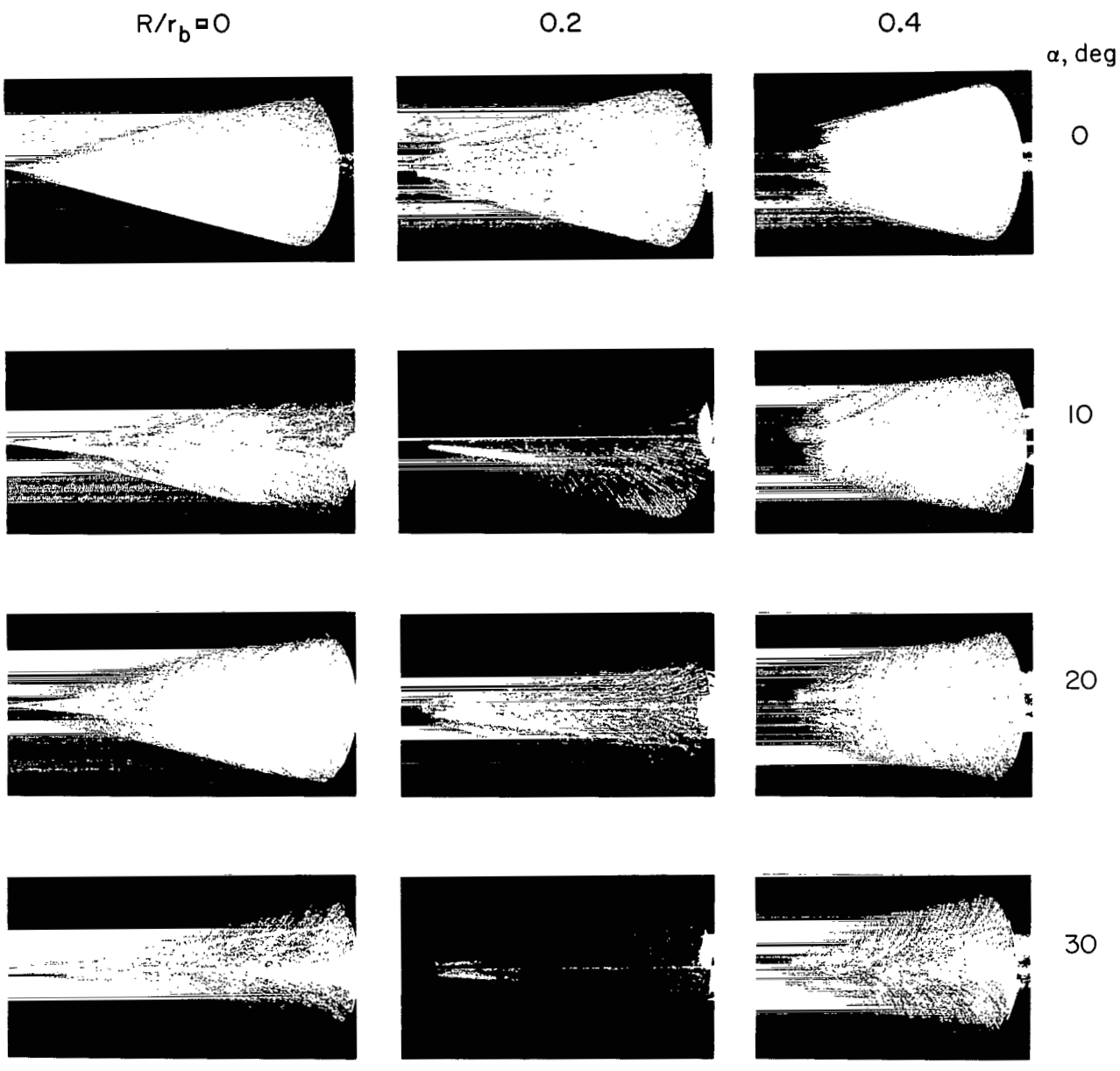


(d) Windward view.

Figure 6.– Concluded.

(a) Top view.

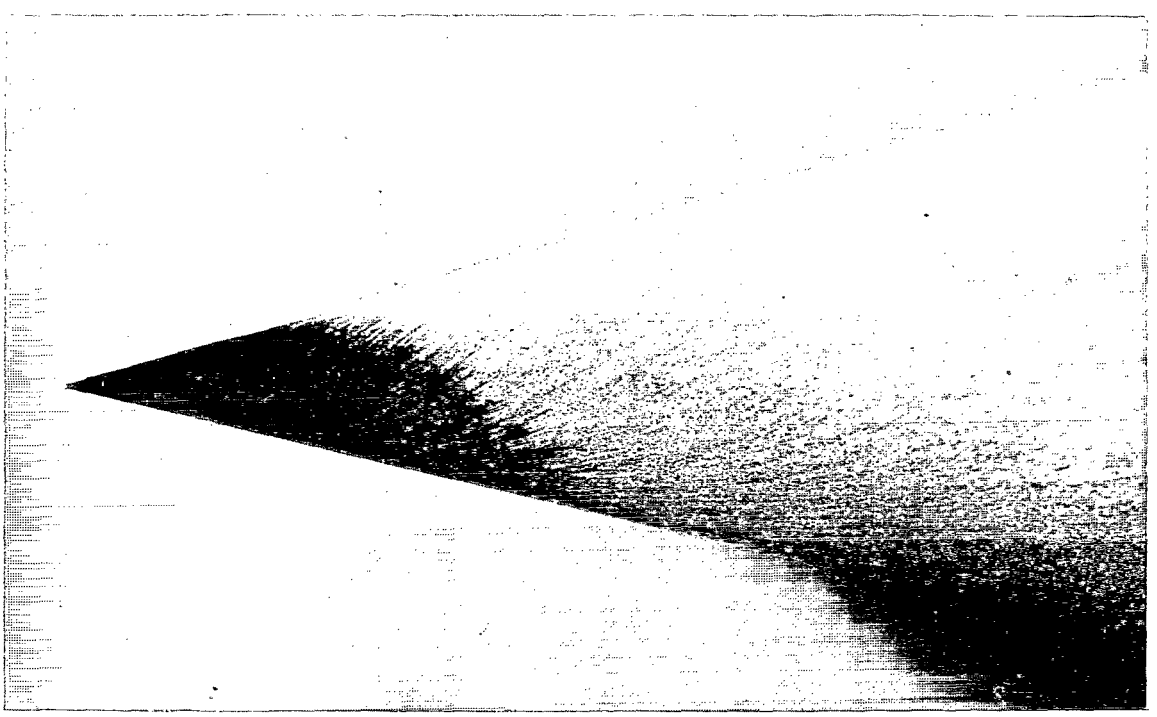

(b) Side view.

Figure 7.– Detailed views of the flow over the cone apex.

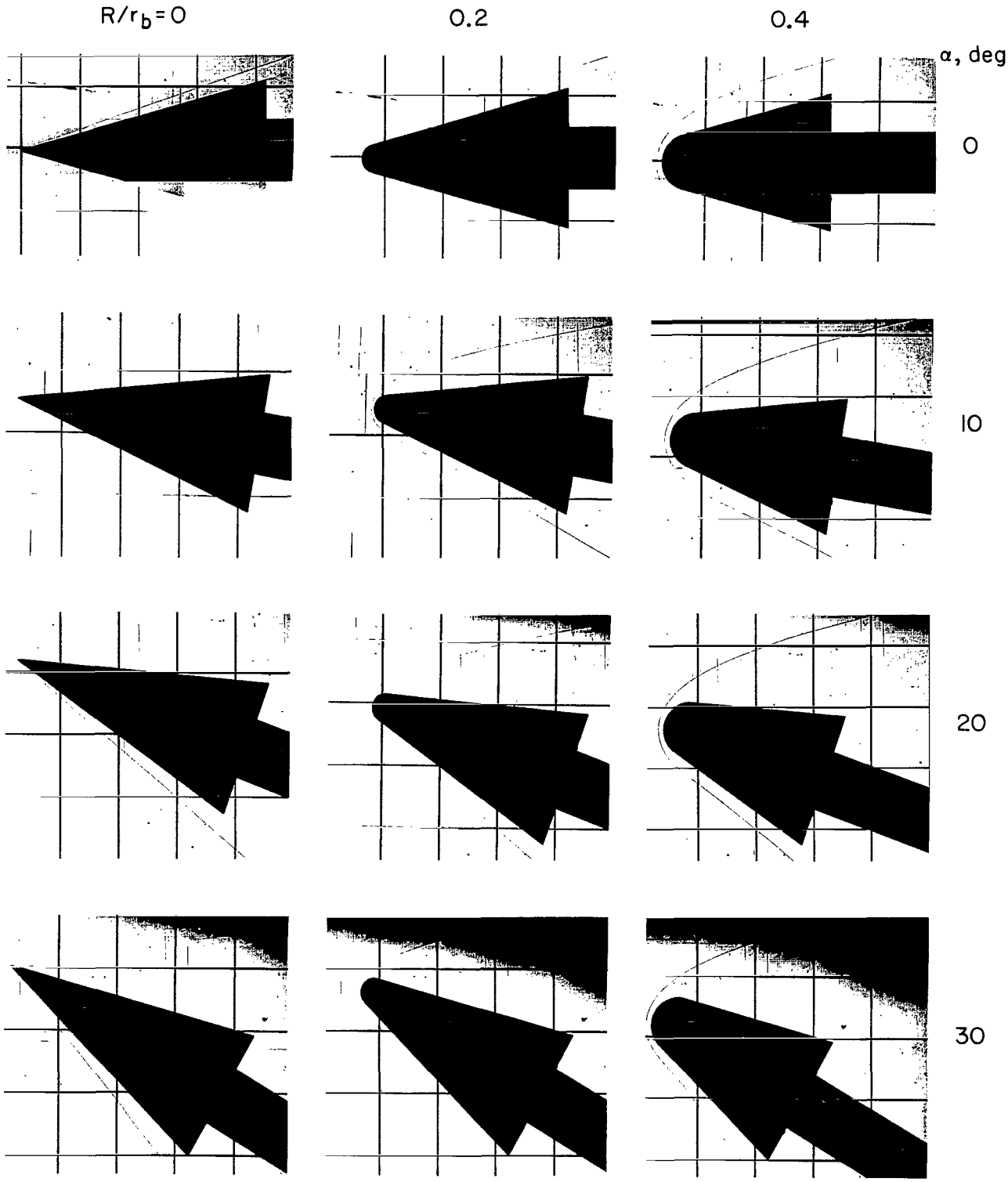


Figure 8.– Effects of angle of attack and bluntness on shock-wave shape; $M_\infty = 14.9$, $Re_\infty = 0.86 \times 10^6$.

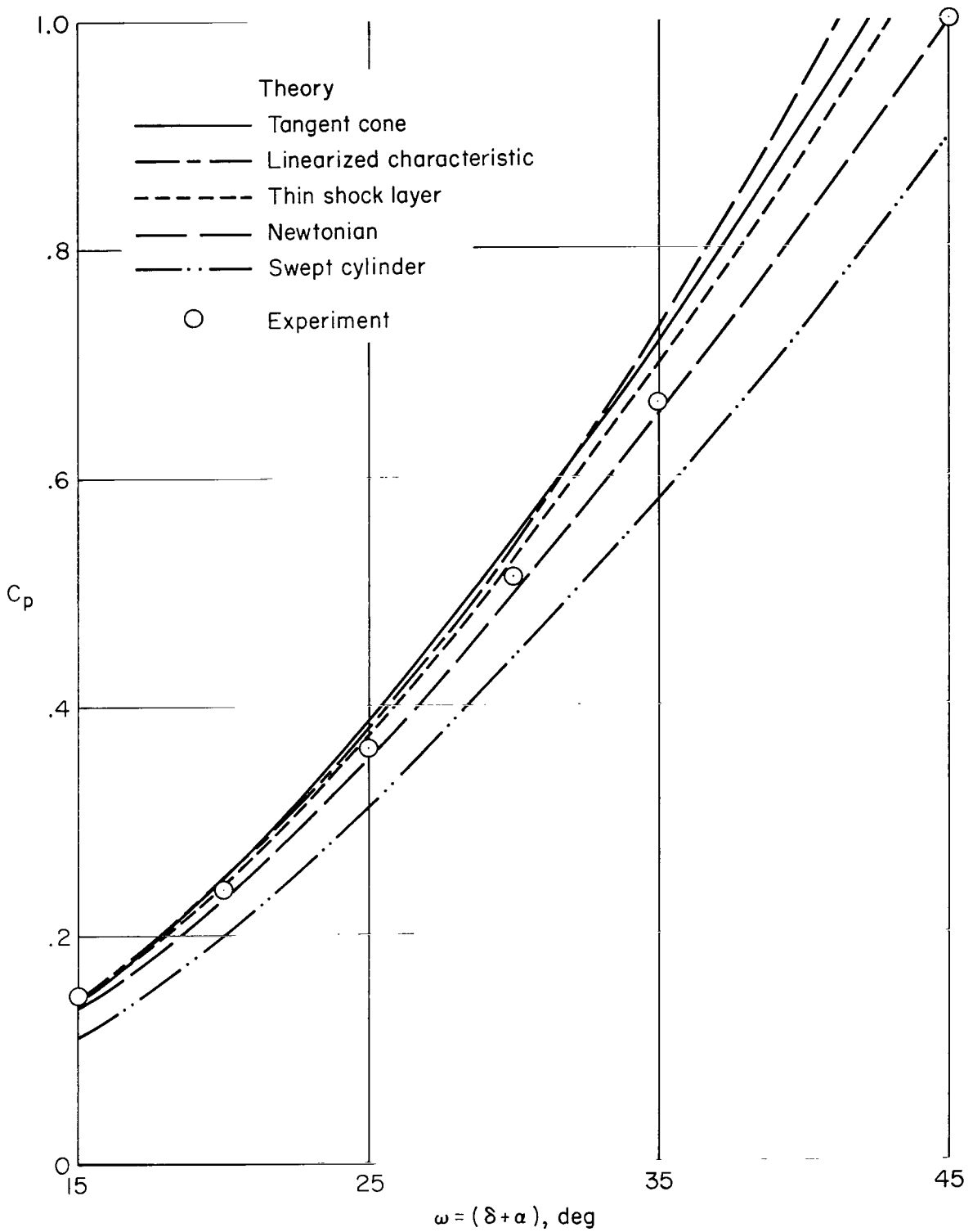


Figure 9.– Comparison of sharp-cone stagnation-line pressure with theory; $M_\infty = 14.9$, $\phi = 180°$, $x_s/L = 0.36$.

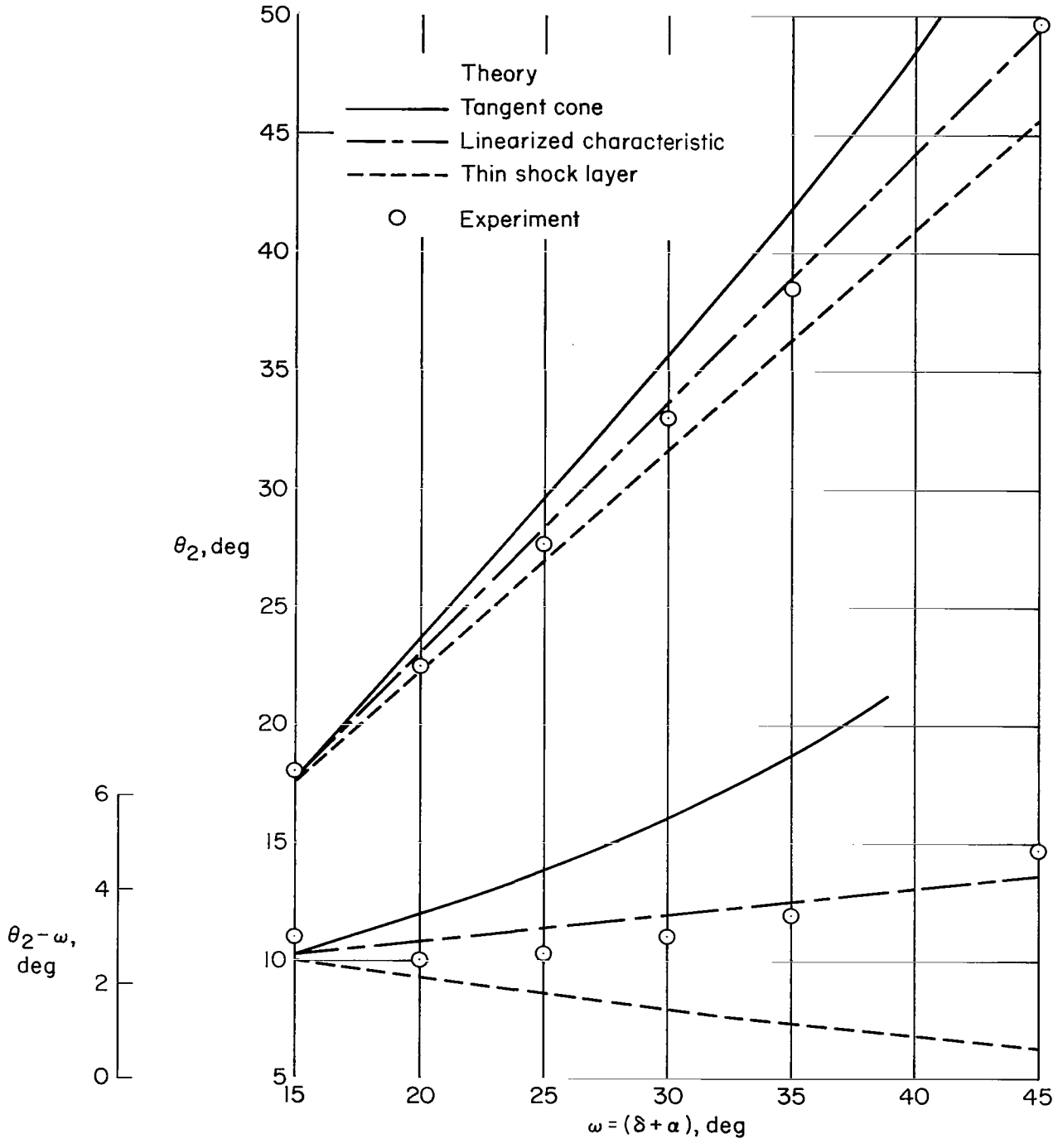


Figure 10.– Comparison of sharp-cone shock angle with theory; $M_\infty = 14.9$, $\phi = 180°$.

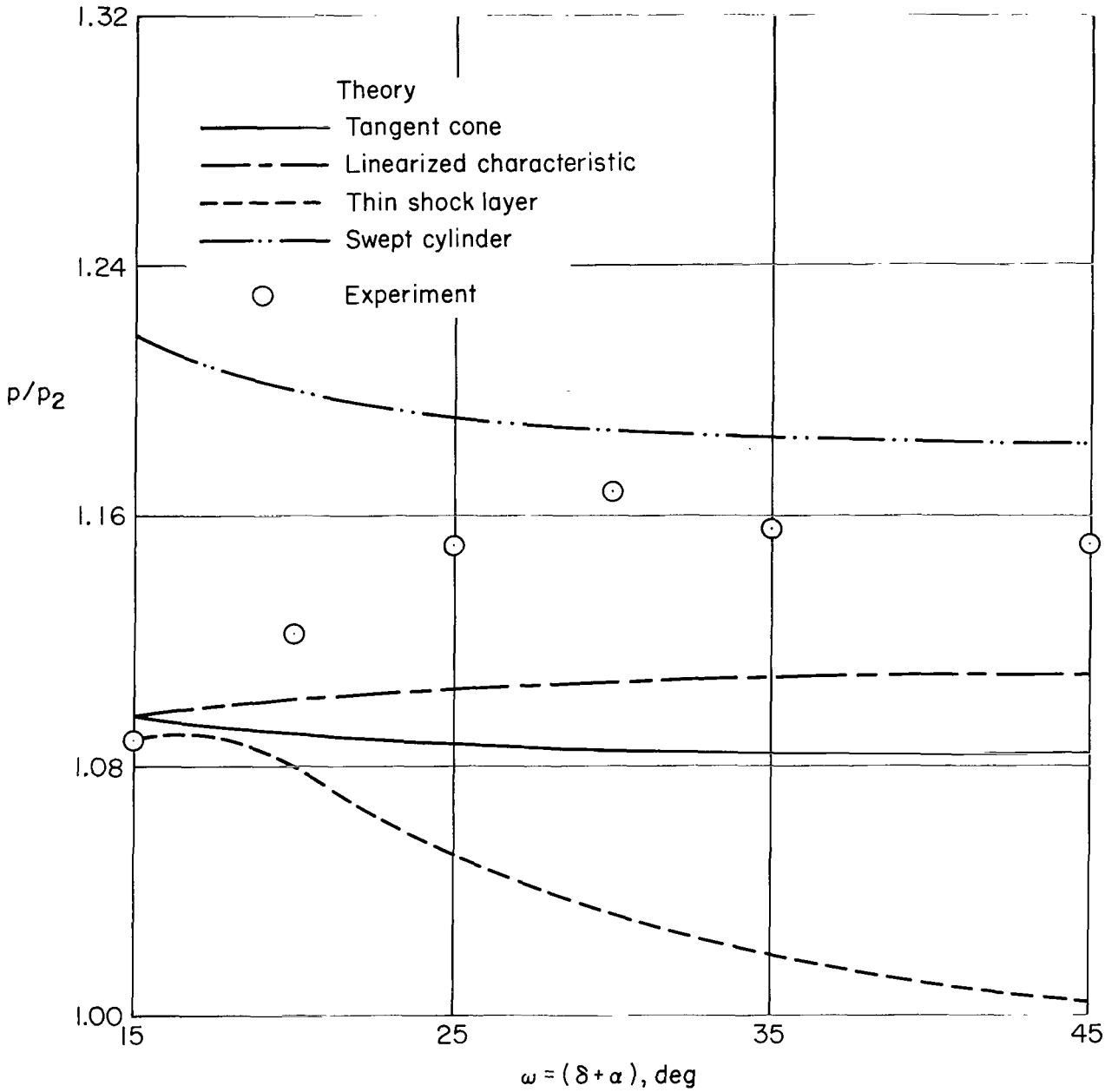


Figure 11.– Comparison of the pressure ratio across the sharp-cone shock layer with theory; $M_\infty = 14.9$, $\phi = 180°$.

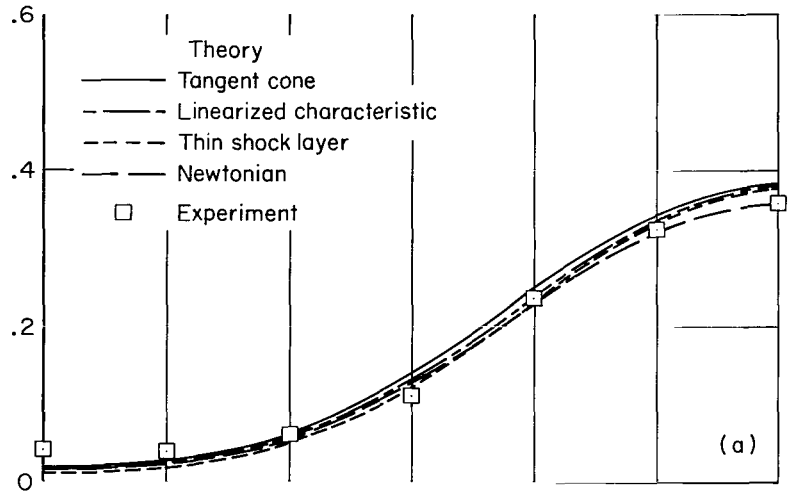


(a) $\alpha = 10°$

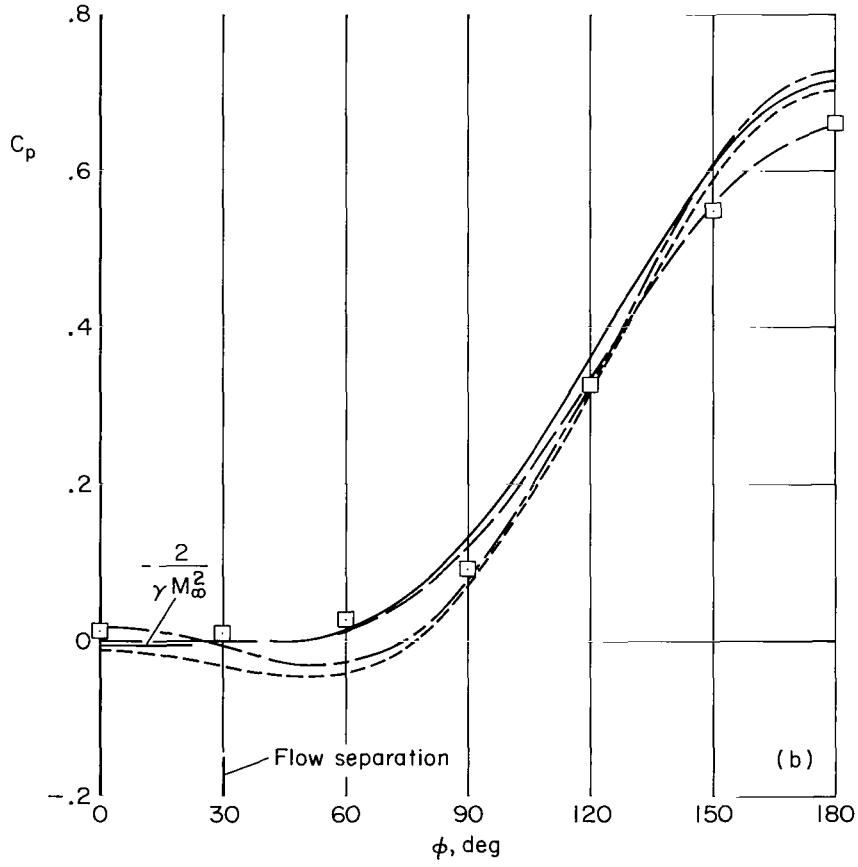


(b) $\alpha = 20°$

Figure 12.– Comparison of sharp-cone circumferential-pressure distribution with theory; $M_\infty = 14.9$.

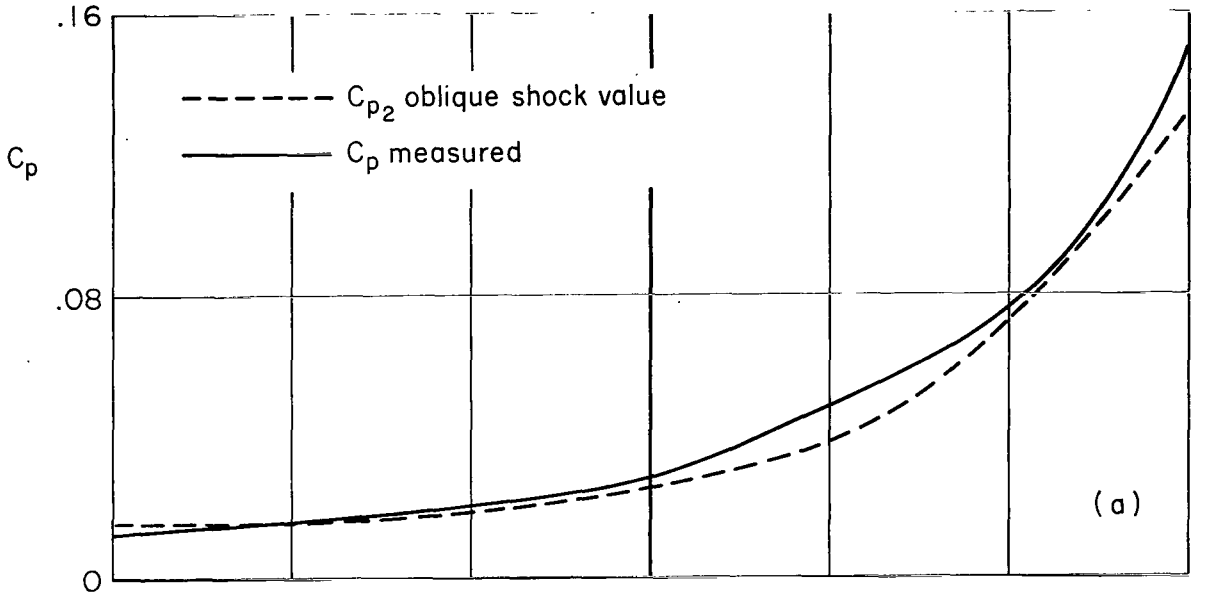


(a) Pressure coefficient.

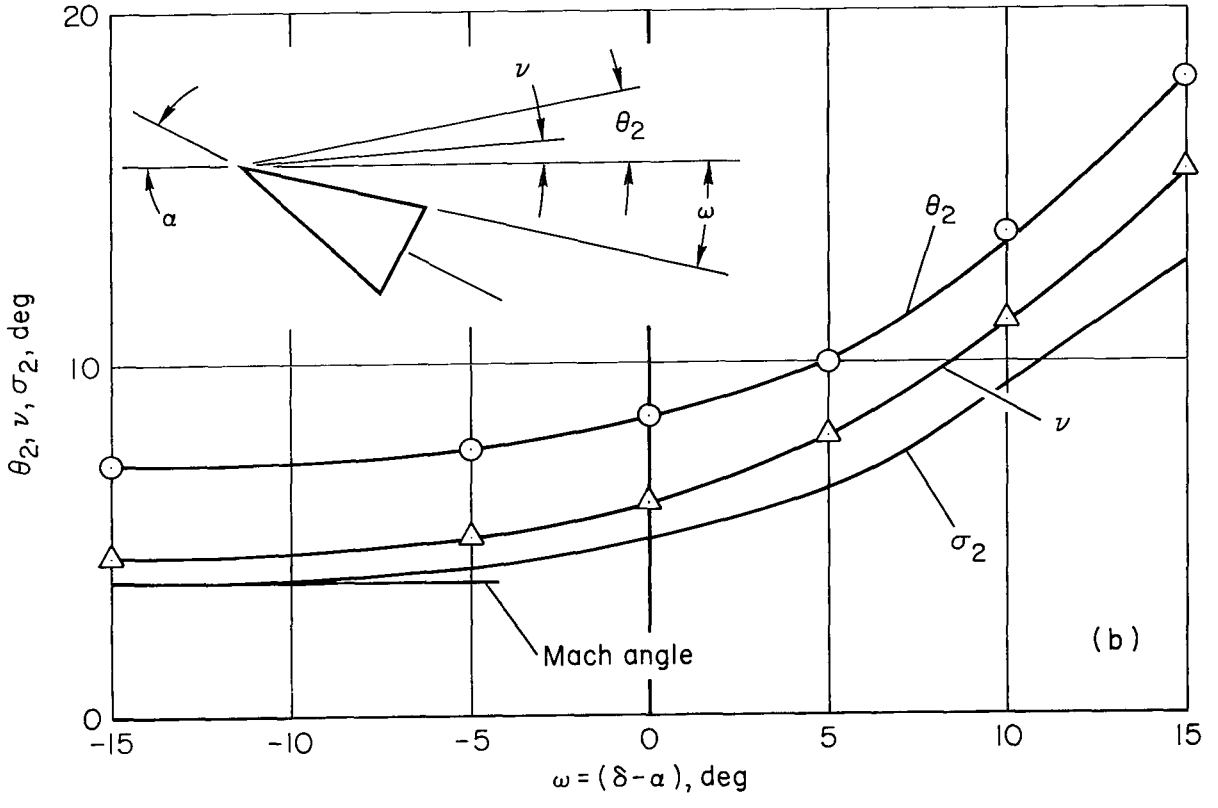


(b) Shock and shear-line angles.

Figure 13.– Characteristics of the flow on the lee side of the sharp cone; $M_\infty = 14.9$, $x_S/L = 0$.

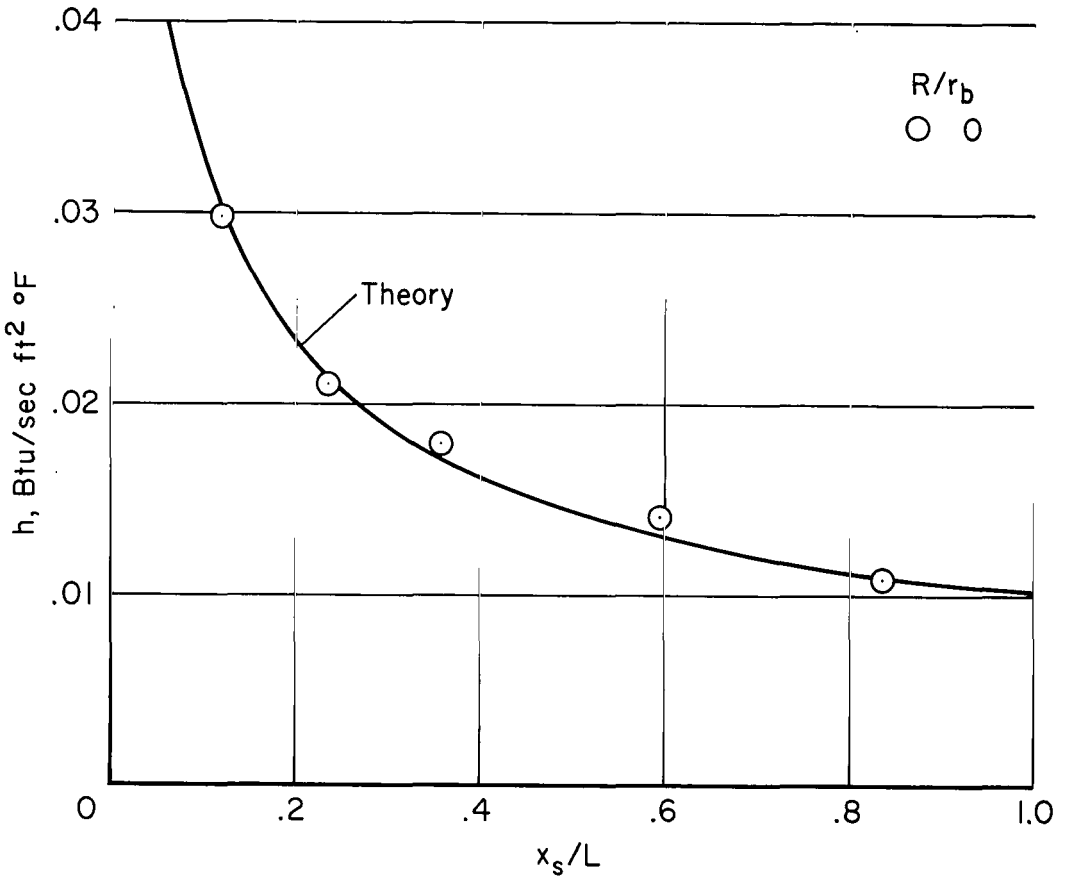


Figure 14.– Comparison of sharp-cone heat-transfer distribution with theory; $M_\infty = 14.9$, $\alpha = 0°$.

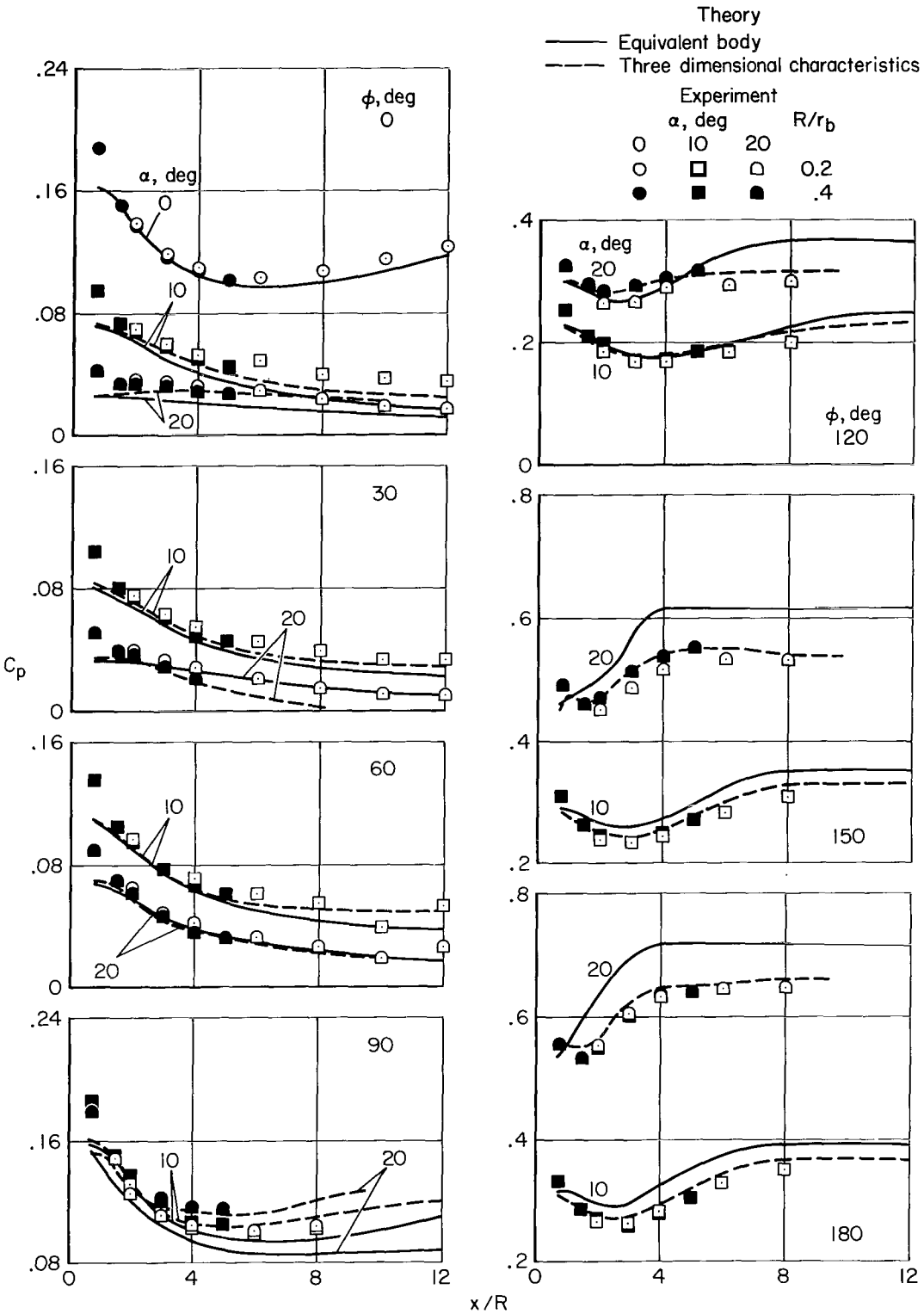


Figure 15.– Comparison of blunt-cone pressure distribution with theory; $M_\infty = 14.9$.

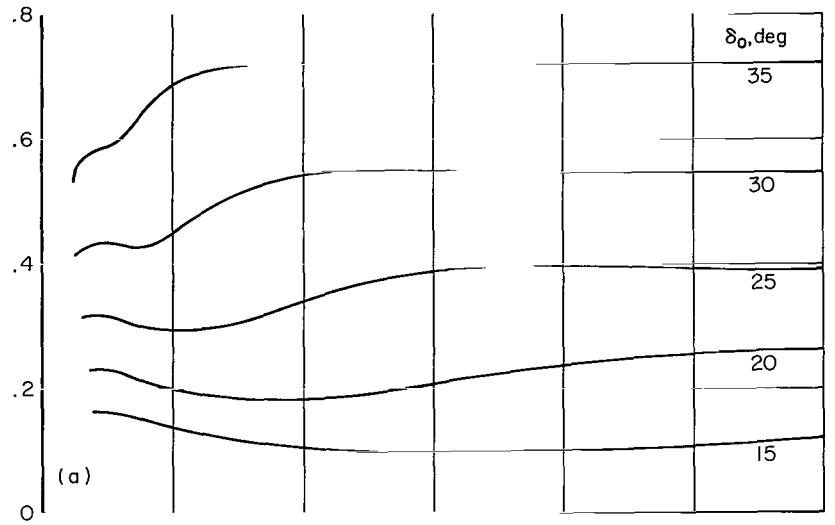


(a) $15° \leqslant \delta_o \leqslant 35°$

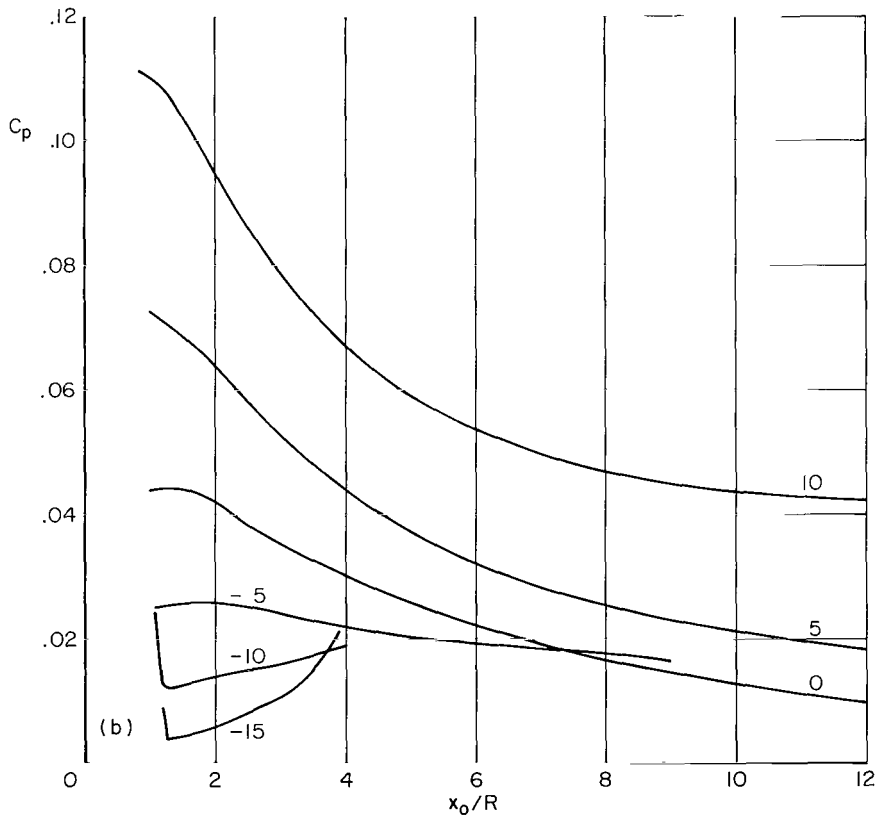


(b) $-15° \leqslant \delta_o \leqslant 10°$

Figure 16.– Effect of varying cone angle on the pressure distribution of blunt cones; $M_\infty = 15$, $\gamma = 1.67$, $\alpha = 0°$.

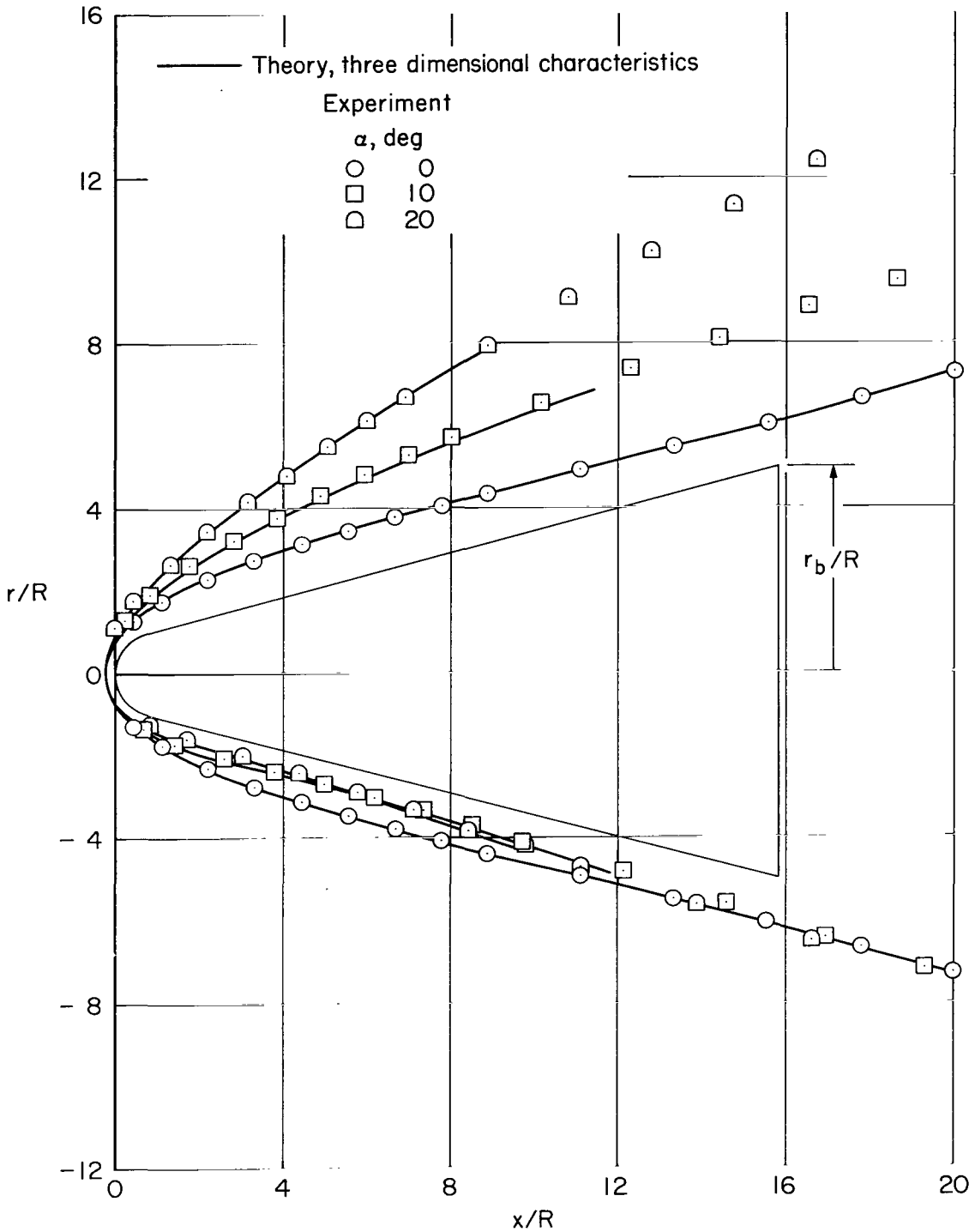


Figure 17.– Comparison of blunt-cone shock-wave shape with theory; $M_\infty = 14.9$.

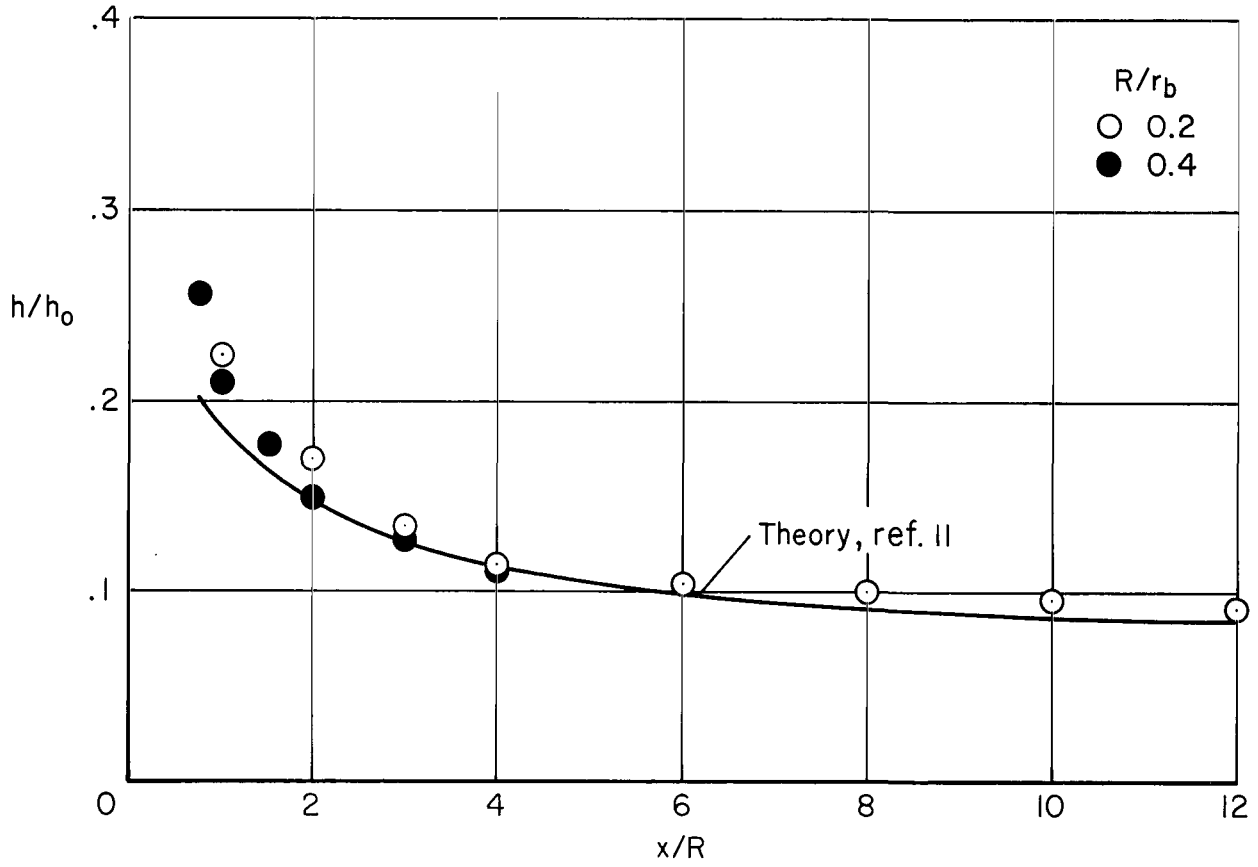


Figure 18.– Comparison of blunt-cone heat-transfer distribution with similarity theory; $M_\infty = 14.9$, $\alpha = 0°$.

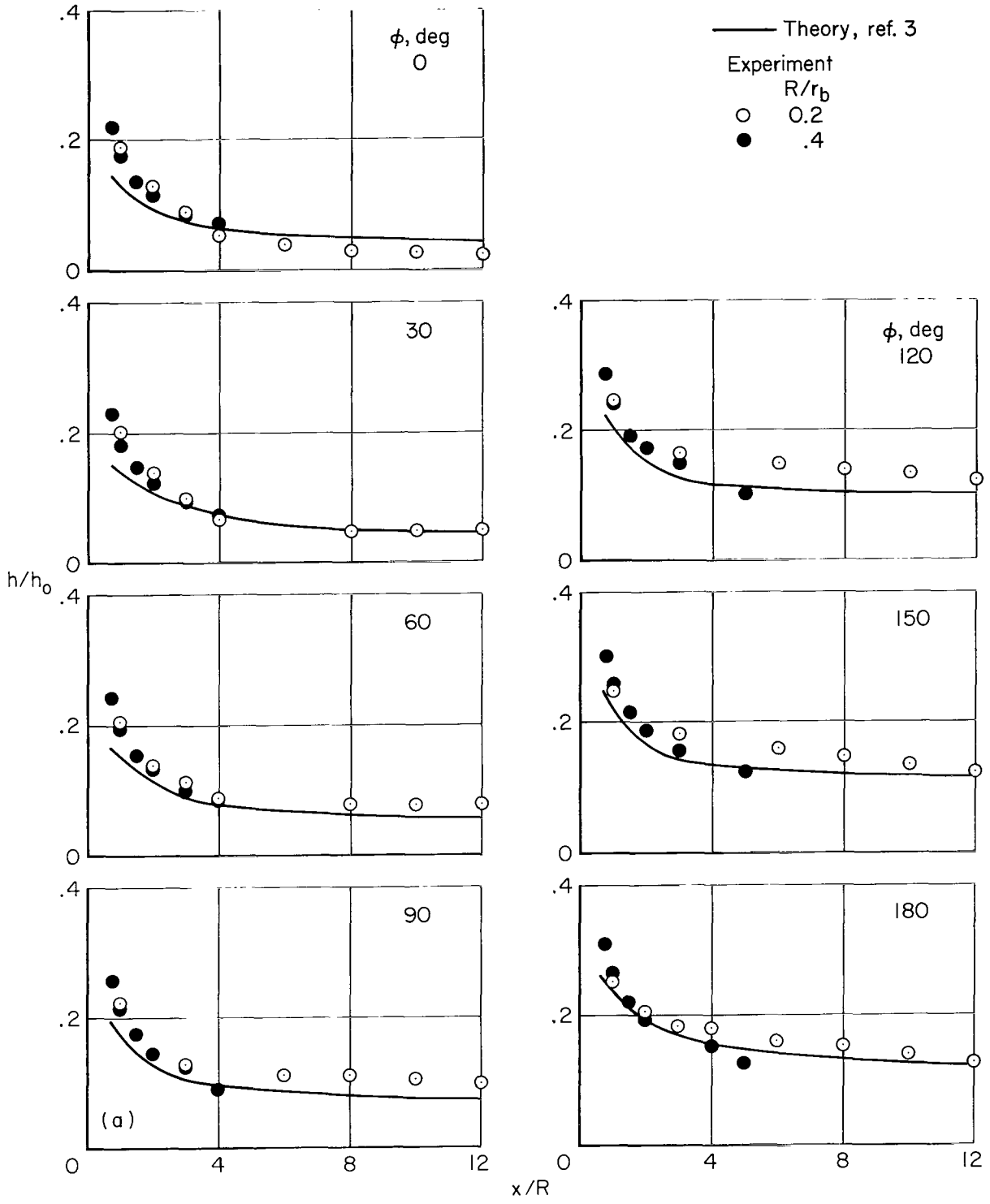


(a) $\alpha = 5°$

Figure 19.- Comparison of blunt-cone heat-transfer distributions with theory; $M_\infty = 14.9$, $\alpha > 0°$.

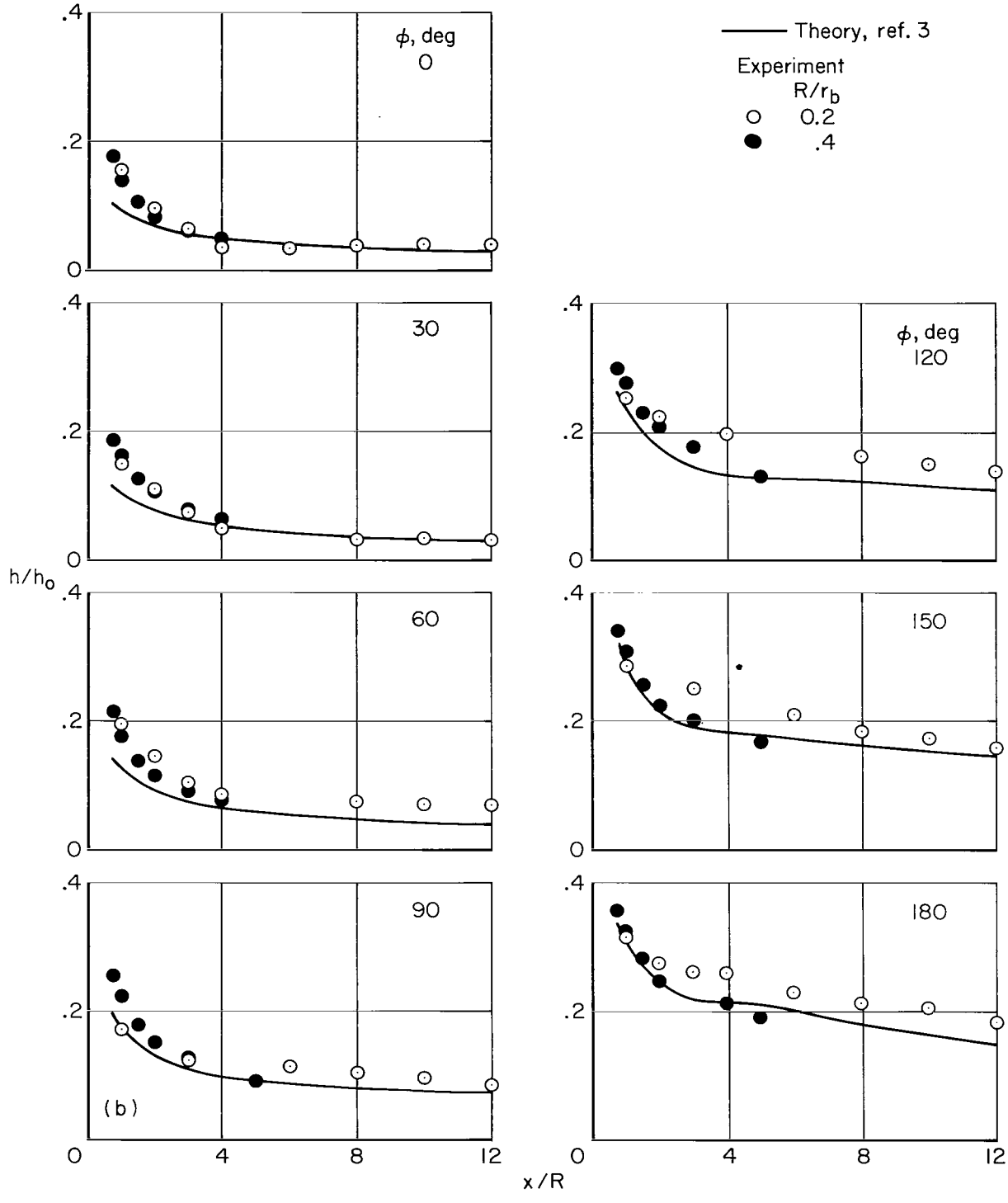


(b) $\alpha = 10°$

Figure 19.– Continued.

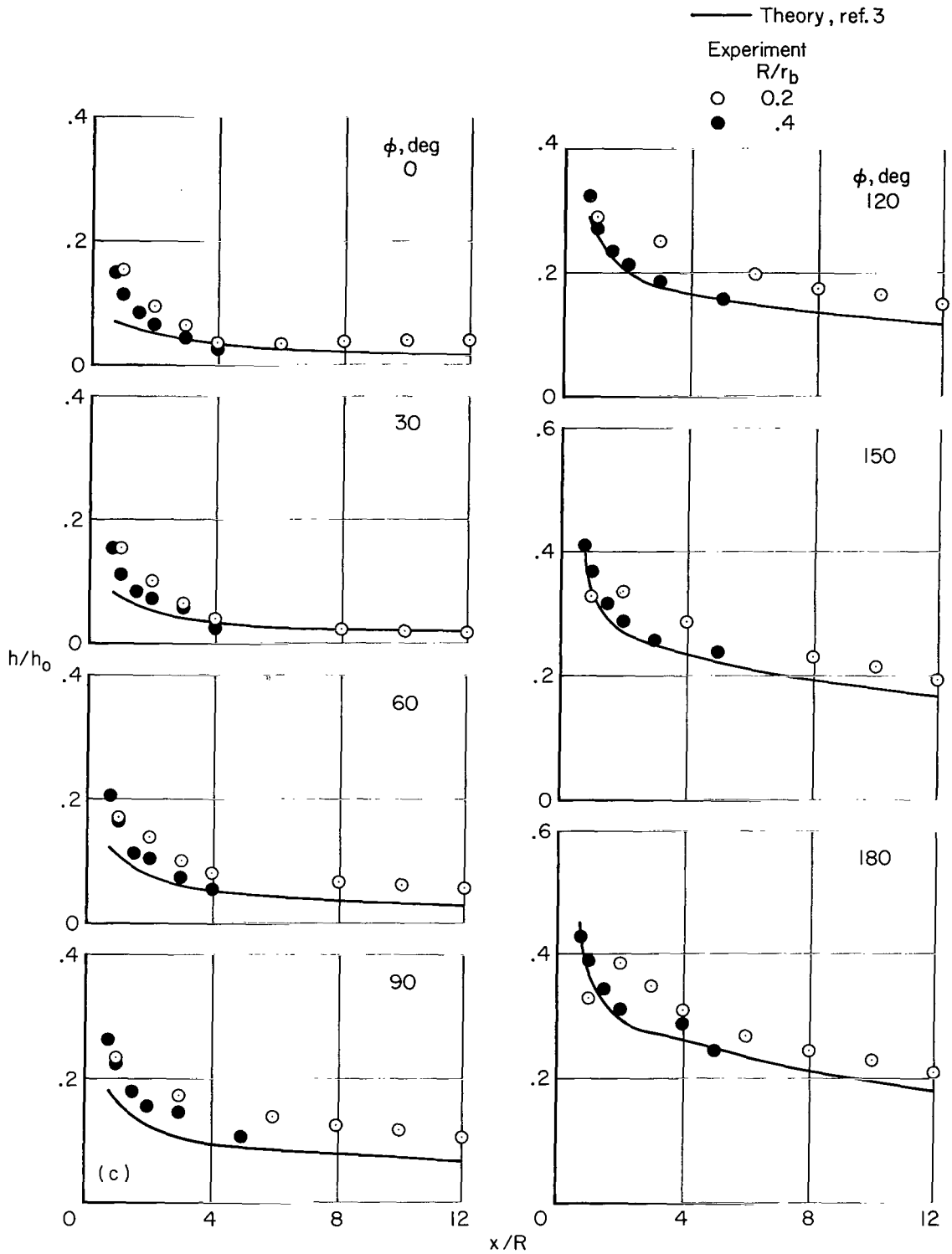


(c) $\alpha = 15°$

Figure 19.– Continued.

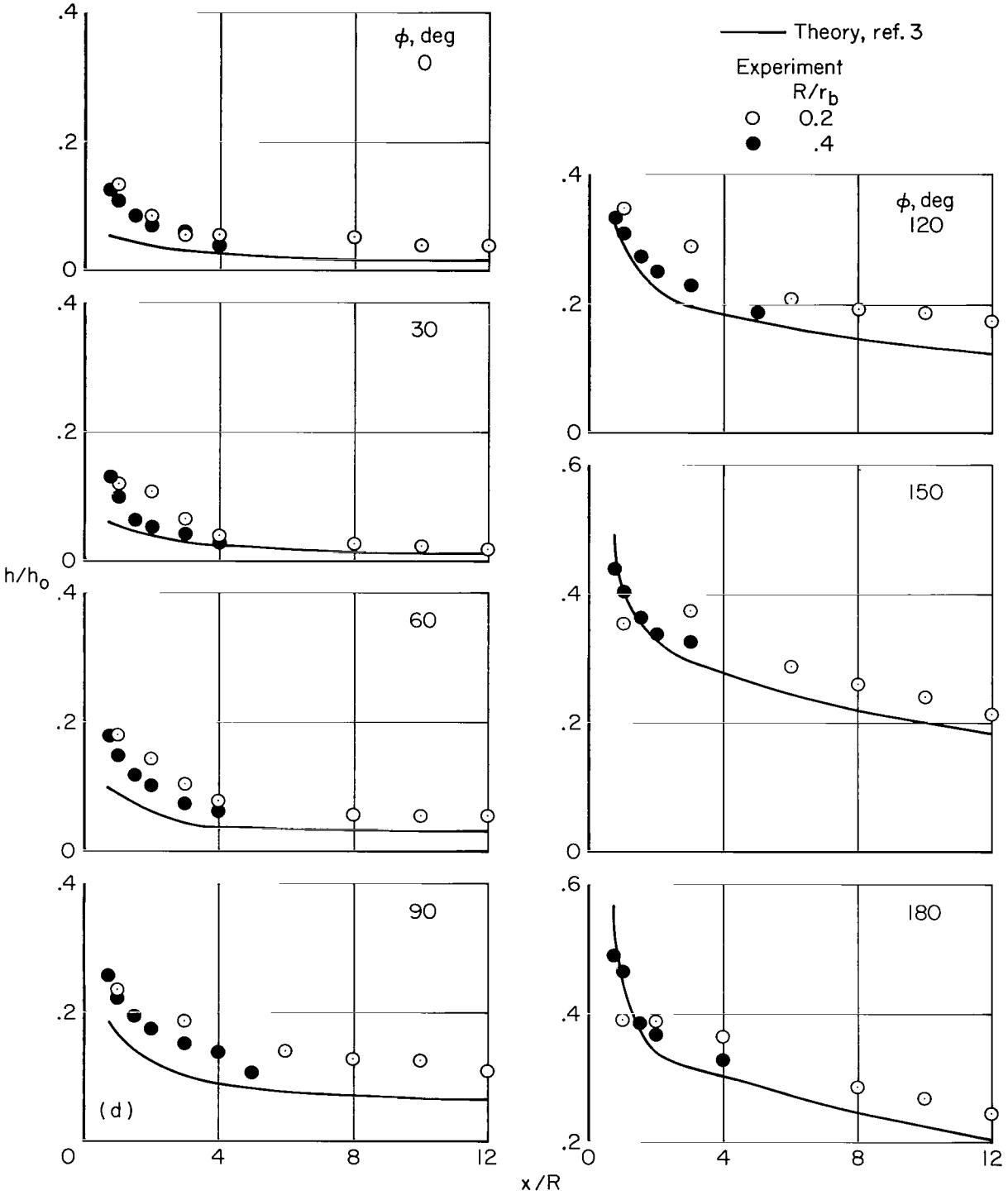


(d) $\alpha = 20°$

Figure 19.– Continued.

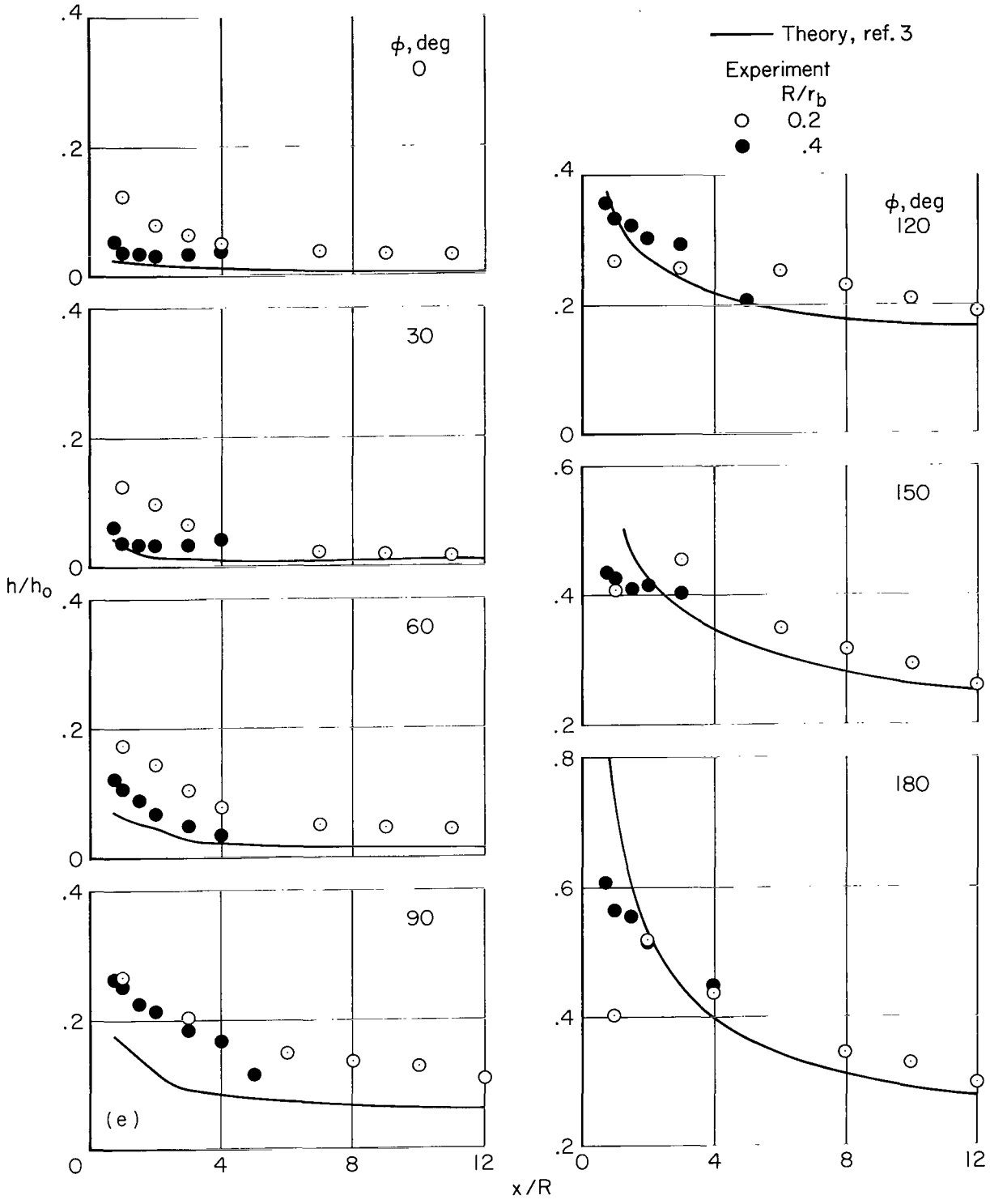


(e) $\alpha = 30°$

Figure 19.– Concluded.



NASA-Langley, 1970 —— 1 A-3566

*"The aeronautical and space activities of the United States shall be conducted so as to contribute . . . to the expansion of human knowledge of phenomena in the atmosphere and space. The Administration shall provide for the widest practicable and appropriate dissemination of information concerning its activities and the results thereof."*

—NATIONAL AERONAUTICS AND SPACE ACT OF 1958

# NASA SCIENTIFIC AND TECHNICAL PUBLICATIONS

TECHNICAL REPORTS: Scientific and technical information considered important, complete, and a lasting contribution to existing knowledge.

TECHNICAL NOTES: Information less broad in scope but nevertheless of importance as a contribution to existing knowledge.

TECHNICAL MEMORANDUMS: Information receiving limited distribution because of preliminary data, security classification, or other reasons.

CONTRACTOR REPORTS: Scientific and technical information generated under a NASA contract or grant and considered an important contribution to existing knowledge.

TECHNICAL TRANSLATIONS: Information published in a foreign language considered to merit NASA distribution in English.

SPECIAL PUBLICATIONS: Information derived from or of value to NASA activities. Publications include conference proceedings, monographs, data compilations, handbooks, sourcebooks, and special bibliographies.

TECHNOLOGY UTILIZATION PUBLICATIONS: Information on technology used by NASA that may be of particular interest in commercial and other non-aerospace applications. Publications include Tech Briefs, Technology Utilization Reports and Notes, and Technology Surveys.

*Details on the availability of these publications may be obtained from:*

**SCIENTIFIC AND TECHNICAL INFORMATION DIVISION**

**NATIONAL AERONAUTICS AND SPACE ADMINISTRATION**

**Washington, D.C. 20546**